Mechanistic interpretation of the effects of acid strength on alkane isomerization turnover rates and selectivity

William Knaeble, Robert T. Carr, Enrique Iglesia *

Department of Chemical and Biomolecular Engineering, University of California, Berkeley, CA 94720, United States

ABSTRACT

Acid strength effects on alkane isomerization turnover rates and selectivities are probed using hexene isomers as reactants on bifunctional catalysts containing tungsten Keggin polyoxometalates (POM) with different central atoms and exhibiting well-defined structures amenable to reliable estimates of deprotonation energies (DPE) as rigorous descriptors of acid strength. Titrations of protons with hindered bases during catalysis and mechanistic interpretations of rate data on POM acids in terms of a common sequence of elementary steps give isomerization rate constants that decrease exponentially with increasing DPE. The sensitivity to acid strength is the same for all interconversions among isomeric hexenes because their respective transition states are similar in the amount and localized character of their cationic charges, which determine, in turn, the extent to which the ionic and covalent interactions that determine DPE are recovered upon formation of ion pairs at transition states. The ratios of rate constants for such interconversions, and thus selectivities, are independent of acid strength and their magnitude merely reflects the stability of the gaseous analogs of their respective transition states on all acids.

© 2014 Elsevier Inc. All rights reserved.

1. Introduction

Catalysis by solid Brønsted acids is ubiquitous in the synthesis and upgrading of fuels and petrochemicals [1]. Rigorous connections between the structure and strength of acid sites and their specific consequences for reactivity and selectivity remain imprecise and often contradictory. Prevailing uncertainties about the number, location, and structure of acid sites during catalysis, the challenges inherent in the unambiguous experimental assessment of acid strength, and measured rates and selectivities that are seldom interpreted in terms of chemical mechanisms have contributed to the pervasive controversies about the strength of acids and about the consequences of acid strength for rates and selectivities of specific reactions and for catalysis in general.

Deprotonation energies (DPE) reflect the ionic and covalent interactions between a proton (H^+) and its conjugate base. These interactions must be overcome to transfer this proton to the intermediates and transition states that mediate transformations catalyzed by acids. DPE values represent a rigorous and probe-independent measure of acid strength; it is accessible to density functional theory (DFT) treatments for well-defined solid acids, such as Keggin polyoxometalate (POM) clusters (1087–1143 kJ mol^{-1} for

$H_{8-n}X^{n+}W_{12}O_{40}$; X = P, Si, Al, or Co in order of increasing DPE) [2, 3] and zeolites with different frameworks [4] and heteroatoms [5].

The effects of DPE, and consequently of acid strength, on alkanol dehydration [3,6,7] and n-hexene isomerization [8] rate constants (per accessible H^+) on Keggin POM clusters ($H_{8-n}X^{n+}W_{12}O_{40}$; X = P, Si, Al, or Co) indicate that the ion-pair transition states (TS) that mediate the kinetically-relevant elementary steps are lower in energy with respect to fully protonated clusters on stronger acids, in part, because of their more stable conjugate anions. Differences in the amount and localization of cationic charge at kinetically-relevant TS relative to those properties for the most abundant surface intermediates (MASI) determine the sensitivity of measured rate constants to acid strength [7,8]. Cations that are small and contain a highly localized charge resemble H^+ and interact most effectively with the conjugate anion [9]; as a result, proton-like TS structures attenuate the effects of acid strength on reactivity most effectively, by recovering most of the energy required to separate the proton. These studies have shown that the effects of acid strength on reactivity reflect differences in interaction energies between the TS and the conjugate anion and those between the MASI species and the conjugate anion.

Here, we assess the effects of acid strength on isomerization turnover rates of hexane and hexene isomers with different backbone structures on bifunctional catalyst mixtures consisting of well-defined Brønsted acids (W-based Keggin POM clusters) and

metal sites (Pt/Al$_2$O$_3$). In such mixtures, Pt sites equilibrate alkanes and alkenes with a given backbone structure via fast hydrogenation–dehydrogenation reactions when such sites are present in sufficient amounts; in such cases, reactant alkenes are present throughout the catalyst mixture at low and constant concentrations; such low concentrations cannot be detected but are known from thermodynamic data at each given temperature and H$_2$ and alkane pressures. These alkenes undergo skeletal isomerization on acid sites and the alkene isomers formed rapidly equilibrate with the respective alkanes upon contact with Pt sites [10–12].

Isomerization rate constants (per H$^+$) were measured for the conversion of 2-methylpentane, 3-methylpentane, 2,3-dimethylbutane, and n-hexane reactants through mechanistic interpretations of rate data and measurements of the number of accessible protons by titrations with organic bases during catalysis. These rate constants reflect TS energies relative to unoccupied Brønsted acid sites and gaseous alkene reactants. Selectivities to isomerization products formed from reactant-derived alkenes after only a single sojourn at an acid site cannot be estimated directly from measured selectivities, because secondary interconversions of alkene products and hydrogenation reactions occur at comparable rates; hydrogenation occurs, either locally within acid domains via hydrogen transfer from alkane reactants or via reactions with H$_2$ after diffusion of alkene isomer products through such acid domains to reach Pt sites. Such selectivities to 3-methylpentene isomer products from 2-methylpentane derived alkenes, which reflect the stability of methyl shift TS relative to those for TS that vary backbone length, were determined—without the use of measured selectivities—from the measured isomerization rate constants for the conversion of each hexane isomer through mechanistic interpretations of rate data. We find that acid strength influences the isomerization rates and selectivities of all skeletal isomers to a similar extent, suggesting that charge distributions are also similar among the ion pairs that mediate each of these reactions. We conclude that the preferential formation of certain isomers reflects the different proton affinities among the gaseous analogs of their respective transition states; these differences and the extent to which deprotonation energies are recovered by interactions of such TS structures with the conjugate anion are not affected, however, by the stability of the conjugate anion and thus do not depend on the strength of the solid acid catalyst.

2. Experimental methods

2.1. Catalyst synthesis and characterization

H$_3$PW$_{12}$O$_{40}$ (Sigma–Aldrich; reagent grade; CAS #12501-23-4), H$_4$SiW$_{12}$O$_{40}$ (Aldrich; >99.9%; CAS #12027-43-9), H$_5$AlW$_{12}$O$_{40}$ (as prepared in [13]), and H$_6$CoW$_{12}$O$_{40}$ (prepared as in [14,15]) were supported on amorphous SiO$_2$ (Cab-O-Sil HS-5; 310 m^2 g^{-1}; 1.5 cm^3 g^{-1} pore volume) by incipient wetness impregnation with ethanol as the solvent. SiO$_2$ was washed three times with 1 M HNO$_3$ and treated in flowing dry air (UHP Praxair; 0.5 cm^3 g^{-1} s^{-1}) at 573 K for 5 h before impregnation. Ethanolic POM solutions (ethanol, Sigma–Aldrich; >99.5%; anhydrous) were added to pretreated SiO$_2$ (1.5 cm^3 solution [g dry SiO$_2$]$^{-1}$) and impregnated samples were stored in closed vials for >24 h before treatment in flowing dry air (UHP Praxair; 0.5 cm^3 g^{-1} s^{-1}) by heating from ambient temperature to 323 K at 0.033 K s^{-1} and holding for 24 h. SiO$_2$-supported POM clusters are denoted as "H$_n$XW/SiO$_2$", where n is the stoichiometric number of protons per cluster and X is the central atom. POM concentrations in the impregnation solutions were set to give a surface density of 0.04 POM [nm-SiO$_2$]$^{-2}$ (~5.0 wt%) for all central atoms, unless noted otherwise. ^{31}P-MAS-NMR spectra of H$_3$PW/SiO$_2$ (Fig. S.1. in Supporting Informa-

tion) confirmed that the procedures used to disperse POM clusters on SiO$_2$ did not alter their Keggin structures. Transmission electron micrographs (Fig. S.2. in Supporting Information) showed that, prior to their exposure to reaction conditions, POM clusters were present as isolated clusters or small two-dimensional oligomers on SiO$_2$ at the surface densities used in this study.

Pt/Al$_2$O$_3$ (1.5 wt%), used as a cocatalyst in physical mixtures with POM/SiO$_2$ Brønsted acids, was prepared by incipient wetness impregnation of γ-Al$_2$O$_3$ (Sasol SBa-200; 193 m^2 g^{-1}, 0.57 cm^3 g^{-1} pore volume) with aqueous H$_2$PtCl$_6$ (Aldrich; CAS #16941-12-1; 0.57 cm^3 g^{-1} dried Al$_2$O$_3$) solution. The γ-Al$_2$O$_3$ was treated in dry air (UHP Praxair; 0.5 cm^3 g^{-1} s^{-1}) at 923 K for 5 h prior to impregnation. The impregnated sample was treated in dry air (Praxair UHP, 0.7 cm^3 g^{-1} s^{-1}) at 383 K for 10 h before heating to 823 K at 0.033 K s^{-1} and holding for 3 h in flowing dry air (Praxair UHP, 0.7 cm^3 g^{-1} s^{-1}). This sample was then treated in H$_2$ (Praxair 99.999%; 0.2 cm^3 g^{-1} s^{-1}) by heating to 723 K at 0.083 K s^{-1} and holding for 2 h. After cooling to 303 K in He (UHP Praxair; 0.7 cm^3 g^{-1} s^{-1}), the Pt/Al$_2$O$_3$ was treated in a dry air/He mixture (2.1% mol O$_2$, 7.9% mol N$_2$, 90% mol He, 0.7 cm^3 g^{-1} s^{-1} total flow) for 2 h.

The Pt dispersion in Pt/Al$_2$O$_3$ (0.92; defined as the fraction of Pt-atoms located at the surfaces of Pt particles) was determined by H$_2$ uptakes at 298 K using a volumetric chemisorption unit and a 1:1 H-atom:Pt$_S$ adsorption stoichiometry (Pt$_S$, surface Pt-atom). Pt/Al$_2$O$_3$ was treated in H$_2$ (99.999% Praxair) at 598 K for 1 h and then held under vacuum at 598 K for 0.5 h before chemisorption measurements. A H$_2$ adsorption isotherm (99.999% Praxair) was measured at 298 K from 0.1 to 50 kPa H$_2$. The cell was then evacuated for 0.25 h at 298 K and a second isotherm was measured under the same conditions. The amount of chemisorbed H$_2$ was calculated from the difference between the first and second isotherms after their respective extrapolations to zero pressure. The Pt dispersion was also determined by CO chemisorption at 298 K using similar pretreatments, a single CO (99.5% Praxair) adsorption isotherm extrapolated to zero pressure, and by assuming a 1:1 CO:Pt$_S$ adsorption stoichiometry (0.78 Pt$_S$/Pt$_{total}$). Their average (0.85) was used to calculate (Pt$_S$/H$^+$) ratios of acid–metal mixtures.

Pt/Al$_2$O$_3$ samples were mixed with POM/SiO$_2$ (P, Si, Al, and Co central atoms) in a mortar and pestle (<100 μm Al$_2$O$_3$ and SiO$_2$ particles) and then pressed into wafers, crushed, and sieved to retain 125–180 μm aggregates. The compositions of these mixtures are reported here as the ratio of Pt$_S$ (from the average dispersion from H$_2$ and CO chemisorption) to accessible H$^+$ (measured by titration during catalysis; Section 3.1.1); this ratio (Pt$_S$/H$^+$) was varied between 6.2 and 22.9 to determine the ratios required to achieve reactant alkane–alkene equilibrium during isomerization catalysis (Section 3.1.2).

2.2. Alkane isomerization rate measurements and titrations with 2,6-di-tert-butylpyridine

2-Methylpentane (2MP), 3-methylpentane (3MP), 2,3-dimethylbutane (23DMB), and n-hexane (nH) isomerization rates were measured on catalyst mixtures (0.01–0.3 g) held within a quartz tubular flow reactor (1.0 cm I.D.) using a porous quartz disk and maintained at 473 K by resistive heating (Watlow Series 982 controller). Temperatures were measured using a K-type thermocouple (Omega; ±0.2 K) held within an indentation at the reactor wall. Mixtures of POM/SiO$_2$ and Pt/Al$_2$O$_3$ were heated to 473 K at 0.083 K s^{-1} in flowing He (UHP Praxair; 0.83 cm^3 s^{-1}) and held for 1 h before catalytic measurements

Liquid 2-methylpentane (Fluka; >99.5% analytical standard), 3-methylpentane (Fluka; >99.5% analytical standard), 2,3-dimethylbutane (Fluka; >99.5% analytical standard), and n-hexane (Fluka; >99.0% GC standard) reactants were evaporated into a flowing He (UHP Praxair) and H$_2$ (99.999% Praxair) stream using a syringe

pump (Cole-Palmer 74900 Series). All transfer lines were kept at 423 K to prevent reactants, products, or titrants from condensing. Flow rates of He and H_2 were metered using electronic mass flow controllers (Porter, Model 201). Molar flow rates of alkanes, H_2, and He were controlled to give desired H_2 pressures and (alkane/H_2) molar ratios and to maintain low reactant conversions (<7%). H_2 pressures between 60 and 90 kPa were used and (alkane/H_2) reactant ratios were varied between 0.01 and 0.3 (higher ratios led to significant deactivation over the course of kinetic experiments). Reactant and product concentrations in the reactor effluent were measured by gas chromatography using flame ionization detection (Agilent 6890N GC; 50 m HP-1 column). All reactant alkanes contained one or more of the product alkanes as impurities (<0.7% carbon selectivity); impurity concentrations were subtracted from those in the reactor effluent when calculating their formation rates. Formation rates of each product were corrected for approach to equilibrium with each reactant using:

$$r_{forward} = r_{net} \left(1 - \left(\frac{P_{prod}}{P_{react}} \right) K_{prod,react}^{-1} \right)^{-1} \qquad (1)$$

in which (P_{prod}/P_{react}) is the ratio of product and reactant pressures within the reactor effluent and $K_{prod,react}$ is their equilibrium constant at 473 K obtained from tabulated thermodynamic data [16]. Moderate catalyst deactivation (<20% over 36 h) occurred on some catalysts during kinetic experiments. All rates were corrected for any intervening deactivation by periodic rate measurements at reference conditions (75 kPa H_2 and 1.9 kPa alkane).

Titration experiments were conducted by dissolving 2,6-di-*tert*-butylpyridine (DTBP, Aldrich; >97%; CAS #585-48-8) in liquid 2MP reactants (between 2.4×10^{-2} and 8.6×10^{-2}% mol) and evaporating this mixture into a flowing H_2/He stream (UHP Praxair; 75% mol H_2) to give DTBP pressures between 0.45 and 2.6 Pa. Isomerization rates and DTBP uptakes at 473 K were calculated from the concentrations of 2MP, its isomerization products, and DTBP in the reactor effluent. Isomerization rates were extrapolated to zero linearly to determine the number of DTBP molecules required to fully suppress isomerization rates. The extrapolated value was assumed to reflect the number of H^+ accessible during catalysis (using a 1:1 H^+:DTBP adsorption stoichiometry) [17].

3. Results and discussion

3.1. 2-Methylpentane, 3-methylpentane, 2,3-dimethylbutane, and n-hexane isomerization turnover rates on POM/SiO₂ mixtures with Pt/Al₂O₃

2-Methylpentane (2MP), 3-methylpentane (3MP), 2,3-dimethylbutane (23DMB), and n-hexane (nH) isomerization turnover rates were measured on SiO₂-supported POM clusters ($H_{8-n}X^{n+}W_{12}O_{40}/SiO_2$) with different central atoms ($X^{n+} = P^{5+}$, Si^{4+}, Al^{3+}, Co^{2+}), each present as physical mixtures with Pt/Al₂O₃ cocatalysts. 2MP isomerization predominantly formed 3MP, 23DMB, and nH products at all conditions and on all catalysts. 2MP isomerization rates were much higher on these bifunctional mixtures than on Pt/Al₂O₃ (by factors >100), indicating that only acid sites contribute to the formation of these isomer products. Measured 2MP isomerization selectivities to 3MP (80–97% for all conditions and catalyst mixtures) were much higher than to 23DMB or nH (0.1–14.5% and 2.3–5.4%, respectively). Traces of 2,2-dimethylbutane (22DMB) were detected (<0.55% carbon selectivity), but its selectivity extrapolated to zero at zero conversion (varied by changing residence time; Fig. S.3., Supporting Information), indicating that 22DMB forms only through secondary reactions of primary isomers along the catalyst bed.

On all catalyst mixtures, 3MP isomerization predominantly formed 2MP (>85% carbon selectivity) and small amounts of 23DMB and nH. Traces of 22DMB were also detected with 3MP reactants (<1.1% carbon selectivity) on these mixtures, but its selectivity also extrapolated to zero at short residence times (Fig. S.4. in Supporting Information). nH isomerization at short residence times on these catalyst mixtures formed 2MP and 3MP in amounts consistent with their interconversion equilibrium (2MP/3MP = 1.4–1.6), much smaller concentrations of 23DMB (<1.0% carbon selectivity), and only traces of 22DMB (<0.1% selectivity). 23DMB reactants on these catalyst mixtures formed predominantly 2MP and 3MP at constant ratios (2MP/3MP = 2.0–2.3), moderate concentrations of 22DMB (∼6% carbon selectivity), and smaller concentrations of nH (<1.0% carbon selectivity) at short residence times. 2MP, 3MP, and nH isomerization formed 22DMB with low selectivities that decreased monotonically with decreasing residence time, indicating that 22DMB forms only from 23DMB-derived alkenes, from which it can form via a single methyl shift along the backbone without the need to increase or decrease the length of the backbone.

These measured selectivities are consistent with elementary isomerization events that only change the number of pendant methyl groups and length of the backbone by one or none when the shifting methyl group is originally attached to tertiary, secondary, or primary carbon atoms, and not at all when the shifting methyl group is originally attached to quaternary carbon atoms. Scheme 1 depicts a reaction network for hexane isomer rearrangements that is consistent with nH forming only from 2MP and 3MP, and 22DMB forming only from 23DMB. According to Scheme 1, comparisons of the absolute and relative stabilities of TS that mediate the interconversions of 2MP, 3MP, nH, and 23DMB, require that we remove the 22DMB formation rate from the measured rate of conversion of 23DMB reactants, which reflect only the stability of the TS for 22DMB and 23DMB interconversion. Thus, 23DMB isomerization rate constants reported here represent the rate of forming mono-branched products, which reflect the stability of the TS that mediate 23DMB conversion to 2MP and 3MP.

3.1.1. Titrations of protons by 2,6-di-tert-butylpyridine (DTBP) during 2-methylpentane isomerization catalysis
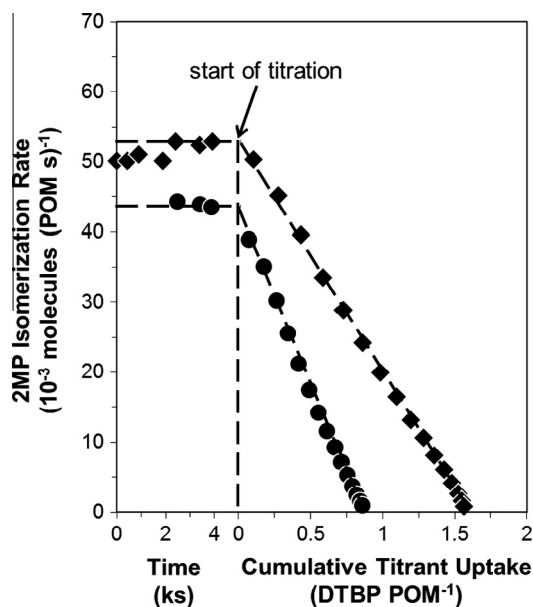
2,6-di-*tert*-Butylpyridine (DTBP) is a selective titrant of Brønsted acid sites because it is protonated irreversibly but cannot coordinate to Lewis acid sites because of steric constraints [17]. Fig. 1 shows 2MP isomerization rates (per POM) as a function of
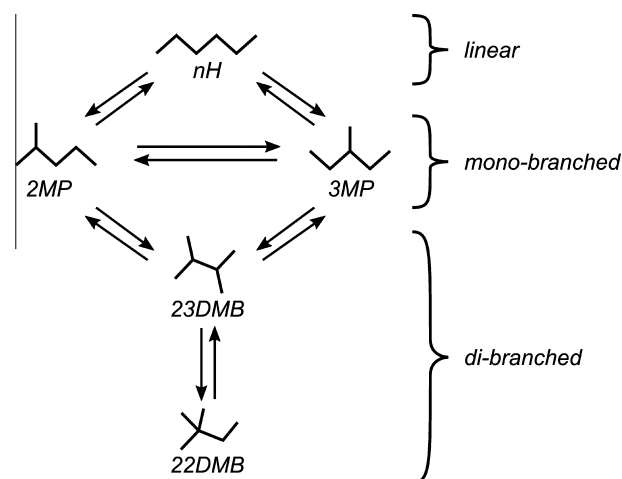
Scheme 1. Isomerization reaction network for gaseous hexane/hexene isomers on POM/SiO₂ mixtures with Pt/Al₂O₃.

time or cumulative DTBP uptake (per POM) before and during DTBP introduction, respectively, on H_3PW/SiO_2–Pt/Al_2O_3 and H_4SiW/SiO_2–Pt/Al_2O_3 mixtures. Isomerization rates decreased linearly with increasing DTBP uptake on both catalysts and reached undetectable levels upon titration of all protons in each sample. These data show that 2MP isomerization occurs only at Brønsted acid sites and that DTBP titrates all protons accessible to reactants. As a result, isomerization turnover rates are reported here as measured rates normalized by the number of protons (H^+) titrated by DTBP in each sample (assuming a 1:1 H^+:DTBP adsorption stoichiometry) during 2MP isomerization catalysis.

The number of titrated H^+ (per POM; Table 1) was smaller than expected from the POM stoichiometry (i.e., $8 - x$ where x is the valence of the central atom) by factors of 2–3.5 for all POM cluster compositions. Secondary structures of POM clusters can prevent DTBP and nonpolar reactants from accessing H^+ located in interstitial spaces within the cubic packing of such secondary structures [8,18], leading to lower DTBP uptakes than expected for isolated fully accessible POM clusters. POM features evident in TEM images of 0.04 POM $(nm-SiO_2)^{-2}$ (<2 nm; Fig. S.2. in Supporting Information) are much smaller than the secondary POM structures that would have had to exist to account for the proton counts shown in Table 1 (~15–20 nm diameters assuming POM anions with 1.2 nm diameters and rhombic dodecahedron secondary structures with bcc crystal structure). Substoichiometric DTBP uptakes may instead reflect intracluster POM dehydroxylation, which removes some H^+ and POM O-atoms as H_2O, or similar reactions between OH groups in POM clusters and surface OH groups on SiO_2 surfaces under the anhydrous conditions of isomerization catalysis [19–21]. Unsupported POM clusters lose H^+ as water at significantly higher temperatures (623 K for $H_3PW_{12}O_{40}$ [22]) than isomerization reaction temperatures (473 K), suggesting that low H^+ counts (Table 1) are caused instead by reactions with silanols. DTPB uptakes varied among $H_3PW_{12}O_{40}/SiO_2$–Pt/Al_2O_3 mixtures containing the same 5 wt% $H_3PW_{12}O_{40}/SiO_2$ catalysts (Table 1) with different amounts of Pt/Al_2O_3, yet their isomerization turnover rates were identical (Fig. 2), indicating that such dehydroxylation reactions do not

Table 1
Number of accessible H^+ per POM cluster measured by chemical titration with 2,6-di-*tert*-butylpyridine[a] during 2-methylpentane isomerization[b] on $HXW_{12}O_{40}/SiO_2$–Pt/Al_2O_3 (X = P, Si, Al, Co) mixtures.

Catalyst	POM content (wt%)	POM surface density (POM nm^{-2})	Accessible H^+ (per POM)
$H_3PW_{12}O_{40}$	5	0.04	0.72[c], 0.73[d], 1.1[e]
$H_3PW_{12}O_{40}$	25	0.20	1.6
$H_4SiW_{12}O_{40}$	5	0.04	1.6
$H_5AlW_{12}O_{40}$	5	0.04	1.45
$H_6CoW_{12}O_{40}$	5	0.04	0.25

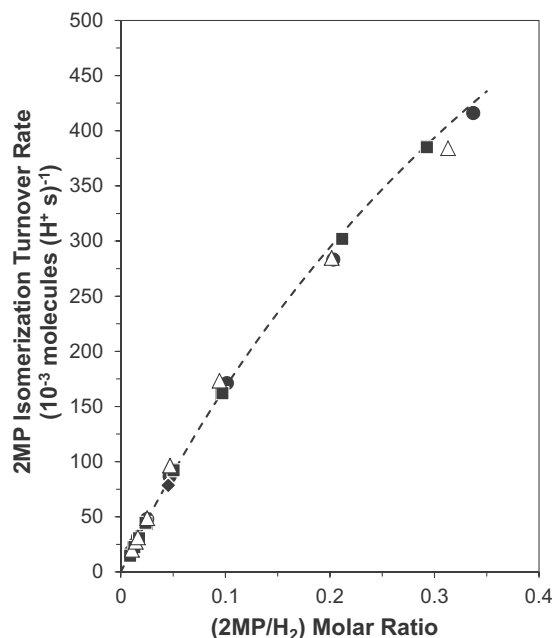[a] Assuming a 1:1 DTBP:H^+ adsorption stoichiometry.
[b] 1.9 kPa 2-methylpentane, 75 kPa H_2, 473 K.
[c] Pt_S/H^+ = 11.7.
[d] Pt_S/H^+ = 6.2.
[e] Pt_S/H^+ = 22.9.

Fig. 2. 2-Methylpentane isomerization turnover rates as a function of (2MP/H_2) ratios on H_3PW/SiO_2–Pt/Al_2O_3 mixtures with (◆) 0.03 H^+ $[nm-SiO_2]^{-2}$ and Pt_S/H^+ = 6.2, (●) 0.03 H^+ $[nm-SiO_2]^{-2}$ and Pt_S/H^+ = 11.7, (△) 0.04 H^+ $[nm-SiO_2]^{-2}$ and Pt_S/H^+ = 22.9, and (■) 0.34 H^+ $[nm-SiO_2]^{-2}$ and Pt_S/H^+ = 10.5 (reaction conditions: 473 K, 0.5 – 25 kPa 2MP, 75 kPa H_2). Dashed lines represent the regression of the data to the functional form of Eq. (4).

influence the reactivity, and by inference the acid strength, of those protons which remain accessible to DTBP. Therefore, we conclude that DTBP uptakes accurately reflect the actual number of accessible Brønsted acid sites *during* catalysis needed to rigorously normalize rates.

3.1.2. Potential effects of diffusional restrictions on isomerization turnover rates and selectivities measured on POM/SiO_2–Pt/Al_2O_3 mixtures

Alkane isomerization rates on bifunctional metal–acid catalysts are limited by the isomerization of alkene intermediates on Brønsted acid sites when (i) the metal function maintains alkane–alkene thermodynamic equilibrium [23] outside of acid domains (defined here as the proton-containing regions devoid of metal sites) and (ii) there are no concentration gradients of reactant-derived alkenes within such acid domains. On such mixtures, transport restrictions do not corrupt measured rates of reactant depletion and calculated rate constants reflect the kinetic and ther-

Fig. 1. 2-Methylpentane isomerization rates (per POM) on (●) H_3PW/SiO_2–Pt/Al_2O_3 (Pt_S/H^+ = 11.7) and (◆) H_4SiW/SiO_2–Pt/Al_2O_3 (Pt_S/H^+ = 4.8) mixtures as a function of time before 2,6-di-*tert*-butylpyridine introduction (473 K, 1.9 kPa 2MP, 75 kPa H_2) and as a function of cumulative titrant uptake (473 K, 1.9 kPa 2MP, 75 kPa H_2, 0.45 Pa DTBP).

Table 2
2-Methylpentane isomerization rate constants ($k_{isom,2}K_{prot,2}$ and $k_{isom,2}$) and protonation equilibrium constants ($K_{prot,2}$) measured on $HXW_{12}O_{40}/SiO_2$–Pt/Al_2O_3 (X = P, Si, Al, Co) mixtures (473 K).

Catalyst	$k_{isom,2}K_{prot,2}$[a,d]	$k_{isom,2}$[b,d]	$K_{prot,2}$[c,d]
$H_3PW_{12}O_{40}$	1759 ± 5	1200 ± 170	1.5 ± 0.2
$H_4SiW_{12}O_{40}$	1159 ± 9	1100 ± 1300	1.0 ± 1.2
$H_5AlW_{12}O_{40}$	771 ± 4	187 ± 11	4.1 ± 0.2
$H_6CoW_{12}O_{40}$	393 ± 3	108 ± 14	3.6 ± 0.5

[a] 10^{-3} molecules (Pa H$^+$ s)$^{-1}$.
[b] 10^{-3} molecules (H$^+$ s)$^{-1}$.
[c] Pa^{-1}.
[d] Errors represent the 95% confidence intervals of parameter in Eq. (4) obtained from the method of least-squares.

Table 3
3MP, 23DMB, and nH isomerization rates measured on H_3PW/SiO_2–Pt/Al_2O_3 mixtures.

Surface density (POM nm^{-2})	Pt$_s$/H$^+$ ratio	3MP turnover rate[a,b]	23DMB turnover rate[a,b]	nH turnover rate[a,b]
0.04	11.7	75	32	7.5
0.04	22.9	80	30	9.4
0.25	10.5	73	32	7.2

[a] 10^{-3} molecules (H$^+$ s)$^{-1}$.
[b] 1.9 kPa alkane, 75 kPa H$_2$, 473 K.

Fig. 3. Isomerization selectivities to 23DMB (●) and nH (■) products for 2MP reactants on H_3PW/SiO_2–Pt/Al_2O_3 (Pt$_s$/H$^+$ = 10.5–11.7; H$^+$ [nm-SiO$_2$]$^{-2}$ = 0.03–0.34) as a function of 2MP pressure (473 K, 0.7–25 kPa 2MP, 75 kPa H$_2$).
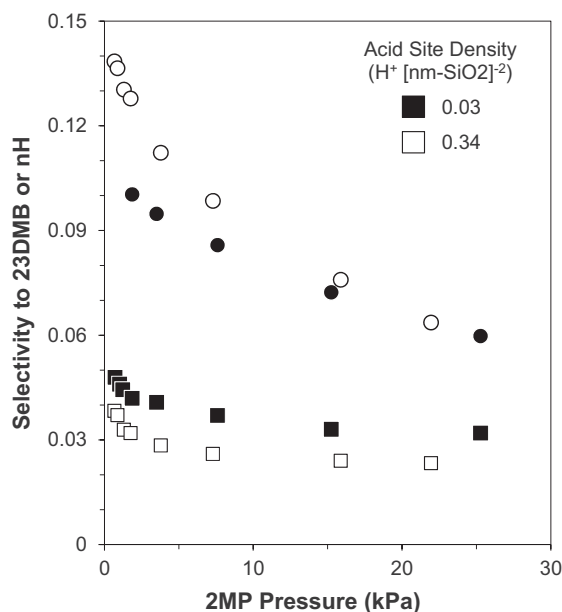
modynamic properties of the acid sites. Next, we confirm that conditions (i) and (ii) are met for the catalyst mixtures studied here.

H_3PW/SiO_2–Pt/Al_2O_3 mixtures with (Pt$_s$/H$^+$) ratios of 6.2, 11.7 and 22.9 gave similar 2MP isomerization turnover rates (per H$^+$) at all conditions (Fig. 2; 0.75–22.5 kPa 2MP, 75 kPa H$_2$). The isomerization turnover rates (per H$^+$) for 3MP, 23DMB, and nH reactants were also unaffected by (Pt$_s$/H$^+$) ratios (Table 3; 1.9 kPa alkane, 75 kPa H$_2$). These results indicate that Pt sites can maintain alkane dehydrogenation–hydrogenation equilibrium for all reactants in these physical mixtures, which contain the POM acid with the highest turnover rate, thus satisfying requirement (i) mentioned above.

Reactant alkene concentration gradients within acid domains were ruled out by the similar measured 2MP, 3MP, 23DMB, and nH isomerization turnover rates on H_3PW/SiO_2–Pt/Al_2O_3 mixtures with very different proton densities (0.03 and 0.34 H$^+$ (nm-SiO$_2$)$^{-2}$) within acid domains (Fig. 2 and Table 3; Pt$_s$/H$^+$ = 10.5 and 11.7, respectively). Any intraparticle concentration gradients of reactant alkenes would have been more severe on samples with higher H$^+$ densities and would have led to concomitantly lower turnover rates, because isomerization rates are nearly proportional to reactant alkene concentrations at the conditions of these experiments [24]. All rate data used to determine kinetic parameters on H_3PW were obtained on samples with 0.03 H$^+$ nm^{-2} acid site densities and a (Pt$_s$/H$^+$) ratio of 11.7 to ensure strict kinetic control and the absence of any diffusional corruptions of measured rates and rate constants.

Bifunctional mixtures with (Pt$_s$/H$^+$) ratios smaller than 11.7 were used for the other POM acids (Pt$_s$/H$^+$ = 4.8, 5.0, and 5.9 for H_4SiW/SiO_2–Pt/Al_2O_3, H_5AlW/SiO_2–Pt/Al_2O_3, and H_6CoW/SiO_2–Pt/Al_2O_3 mixtures, respectively), which have lower isomerization turnover rates than H_3PW/SiO_2–Pt/Al_2O_3 mixtures (Fig. 4). Such ratios were chosen to avoid any contributions to rates from Pt-catalyzed isomerization reactions (Section 3.1). These mixtures have (Pt$_s$/H$^+$) ratios similar to (and isomerization turnover rates lower than) the H_3PW/SiO_2–Pt/Al_2O_3 mixture with a (Pt$_s$/H$^+$) ratio of 6.2, for which such ratios were sufficient to maintain alkane dehydrogenation–hydrogenation equilibrium for 2MP reactants, sug-

gesting that the metal function in these samples are also sufficient to maintain alkane–alkene equilibrium outside acid domains. Transport restrictions within acid domains for reactant alkenes would have been less severe for these other POM acids supported with 0.04 POM (nm-SiO$_2$)$^{-2}$ surface densities (which were used for kinetic experiments) than for the H_3PW/SiO_2 sample with a 0.20 POM (nm-SiO$_2$)$^{-2}$ surface density, because they have much lower isomerization rates than the H_3PW/SiO_2 sample when normalized by the pellet volume of the silica support (~8–140 fold), yet similar diffusion rates because of the similar size and porous structure of the silica domains that contain the acid sites. Thus, isomerization turnover rates measured on these H_4SiW/SiO_2–Pt/Al_2O_3, H_5AlW/SiO_2–Pt/Al_2O_3, and H_6CoW/SiO_2–Pt/Al_2O_3 mixtures are not corrupted by transport restrictions.

Measured alkane isomerization selectivities on bifunctional metal–acid catalysts reflect the relative rates of product formation from reactant alkenes after only a single sojourn at an acid site only when rates of secondary interconversions of alkene products are much lower than their respective hydrogenation rates, either locally within acid domains via hydrogen transfer from alkane reactants or via reactions with H$_2$ after their diffusion through such acid domains to reach Pt sites. Only on such mixtures, transport restrictions would not corrupt measured selectivities and calculated rate constants for *individual* product formation would rigorously reflect the kinetic and thermodynamic properties of the isomerization TS that mediates each respective formation reactions. Selectivities measured on such mixtures at differential conditions are expected to be independent of rates of product alkene hydrogenation and, consequently, reactant alkane pressure. Fig. 3 shows 2MP isomerization selectivities to 23DMB ($S_{meas,23}$) and nH ($S_{meas,nH}$) products as a function of 2MP pressure and 75 kPa H$_2$ on H_3PW/SiO_2–Pt/Al_2O_3 mixtures with very different acid site densities (0.03 and 0.34 H$^+$ (nm-SiO$_2$)$^{-2}$). $S_{meas,23}$ and $S_{meas,nH}$ values decrease with increasing 2MP pressure on these samples suggesting they depend, to some extent, on rates of product alkene hydrogenation via hydride transfer from alkane reactants. Increasing 2MP pressure increases rates of hydrogenation locally within acid domains, decreasing the concentration of product alkenes in such acid domains and, concomitantly, rates of secondary inter-
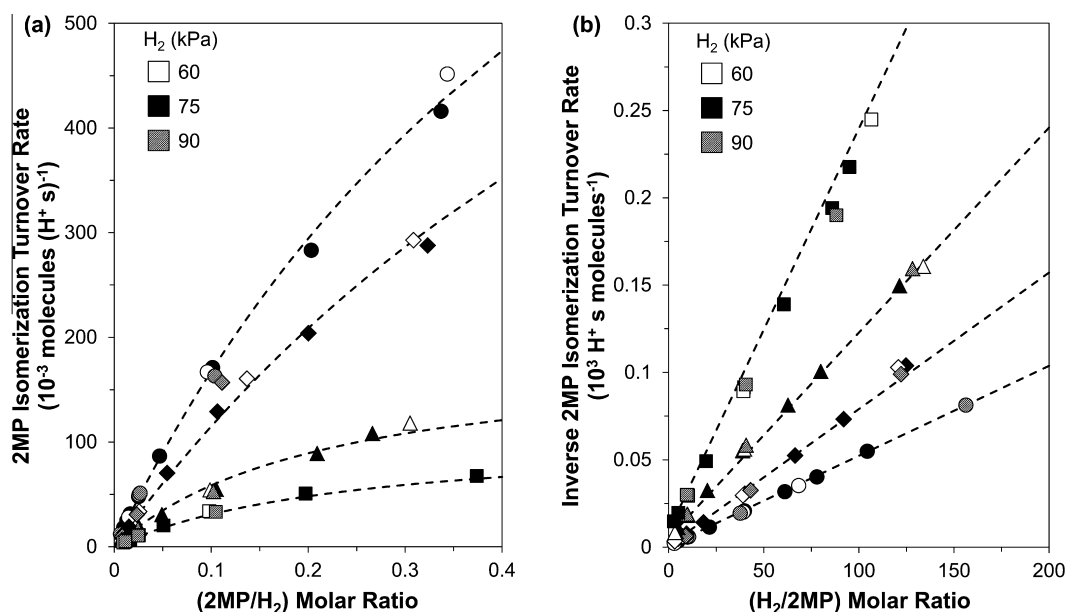
Fig. 4. (a) 2-Methylpentane isomerization turnover rates as functions of the (2MP/H$_2$) ratio and (b) inverse 2-methylpentane isomerization turnover rates as a function of the (H$_2$/2MP) ratio on mixtures of Pt/Al$_2$O$_3$ with (●) H$_3$PW/SiO$_2$ (Pt$_S$/H$^+$ = 11.7), (◆) H$_4$SiW/SiO$_2$ (Pt$_S$/H$^+$ = 4.8), (▲) H$_5$AlW/SiO$_2$ (Pt$_S$/H$^+$ = 5.0), and (■) H$_6$CoW/SiO$_2$ (Pt$_S$/H$^+$ = 5.9) (reaction conditions: 473 K, 0.5–25 kPa 2MP, 60–90 kPa H$_2$). Dashed lines represent the regression of the data to the functional form of Eq. (4).

conversions of alkene products. $S_{meas,nH}$ values in Fig. 3 appear to approach constant values at high 2MP pressures (>10 kPa) suggesting that at such high 2MP pressures increasing rates of hydrogenation locally within acid domains is not effective at changing the net rate of secondary interconversions among 3MP and nH derived alkene products. Decreasing the acid site density of the H$_3$PW/SiO$_2$–Pt/Al$_2$O$_3$ mixtures, which decrease rates of secondary interconversions and hydrogenation via hydride transfer from alkane reactants within such domains but not the rates of diffusion of product alkenes through acid domains, gave higher $S_{meas,nH}$ values (by 1.4 factors) at high 2MP pressures (>10 kPa in Fig. 3). These data indicate that transport restrictions indeed influence measured selectivities on these samples for the range of 2MP and H$_2$ pressures in Fig. 3 (including 2MP pressures >10 kPa); as a result, secondary interconversions of alkene products at these conditions occur at rates similar to their hydrogenation, both locally within acid domains via hydrogen transfer from alkane reactants and via reactions with H$_2$ after their diffusion through such acid domains to reach Pt sites. In such cases, rates and selectivities for isomerization reactions to *individual* primary products (defined as those formed from reactant alkenes in one surface sojourn) cannot be inferred directly from measured selectivities. These constraints preclude the determination of such *individual* product formation rates for most of the isomer products formed; as we show in Section 3.1.3, such formation rates and, as a result, selectivities for 3-methylpentene formation as a primary product from 2-methylpentene can be determined explicitly for any given catalyst mixture from measured isomerization turnover rates for 2MP, 3MP, 23DMB, and nH reactants. Next, such isomerization turnover rates measured on H$_3$PW/SiO$_2$–Pt/Al$_2$O$_3$, H$_4$SiW/SiO$_2$–Pt/Al$_2$O$_3$, H$_5$AlW/SiO$_2$–Pt/Al$_2$O$_3$, and H$_6$CoW/SiO$_2$–Pt/Al$_2$O$_3$ mixtures are interpreted mechanistically.

3.1.3. Mechanistic interpretation of isomerization turnover rate data for POM/SiO$_2$–Pt/Al$_2$O$_3$ mixtures

Fig. 4a shows 2MP isomerization turnover rates (per H$^+$) as a function of (2MP/H$_2$) ratio (a surrogate for the concentration of the alkene regioisomers with the 2-methyl backbone in equilibrium with 2MP reactants) on POM/SiO$_2$–Pt/Al$_2$O$_3$ mixtures with

P, Si, Al, and Co central atoms ((Pt$_S$/H$^+$) = 4.8–11.7). 2MP isomerization turnover rates (at a given reaction condition) increased as the valence of the POM central atom increased. Turnover rates also increased with increasing (2MP/H$_2$) ratios on each sample, linearly at first and then more gradually at higher reactant ratios (Fig. 4a). 2MP isomerization rates depend only on (2MP/H$_2$) ratios and not on the individual values of the 2MP or H$_2$ pressures (60–90 kPa H$_2$) used to obtain these ratios on all POM/SiO$_2$–Pt/Al$_2$O$_3$ mixtures.

The elementary steps in Scheme 2 may be used to derive a rate equation consistent with these measured effects of (2MP/H$_2$) ratios on isomerization rates, as shown previously for other bifunctional isomerization catalysts [8,23,25]. Pt sites equilibrate 2MP with all 2-methylpentene regioisomers (Scheme 2, Step 1 illustrated for the case of 2-methylpent-2-ene); as a result, alkene pressures are proportional to (2MP/H$_2$) ratios and to their respective dehydrogenation equilibrium constants ($K_{dehy,2}$). Quasi-equilibrated protonation of 2-methylpentene isomers at acid sites forms adsorbed 2-methylpentoxide isomers with backbone attachments to surfaces at locations prescribed by their relative thermodynamic stability (Scheme 2, Step 2 shown for 2-methylpent-2-ene and 2-methylpent-3-oxide). Adsorbed 2-methylpentoxides then isomerize in irreversible steps to alkoxides with a different backbone structure (Scheme 2, Step 3 for the case of 3-methylpent-2-oxide). These backbone rearrangements are mediated by cationic TS that resemble cyclopropyl carbenium ions (or cyclobutyl carbenium ions for interconversions of 3-methylpentoxides and 2,3-dimethylpentoxides) in which C–C bonds (and C–H bonds, for cyclopropyl carbenium ion TS that change the number of pendant methyls) cleave and form in concerted steps [26–30]. Product alkoxides either deprotonate to form their gaseous alkenes (Scheme 2, Step 4 shown for 3-methylpent-2-ene) or hydrogenate via hydrogen transfer from 2MP to form their respective gaseous alkane isomer and a 2-methylpentoxide (Scheme 2, Step 5 shown for 3-methylpent-2-oxide and 2-methylpent-3-oxide). Gaseous alkene products may re-protonate at acid sites (Scheme 2, Step 4) or diffuse to Pt sites and undergo hydrogenation reactions with H$_2$ to form the respective gaseous alkane isomer (Scheme 2, Step 6 shown for 3MP). Alkenes (and alkoxides) with a given backbone but different double-bond positions can be rigorously treated in all kinetic
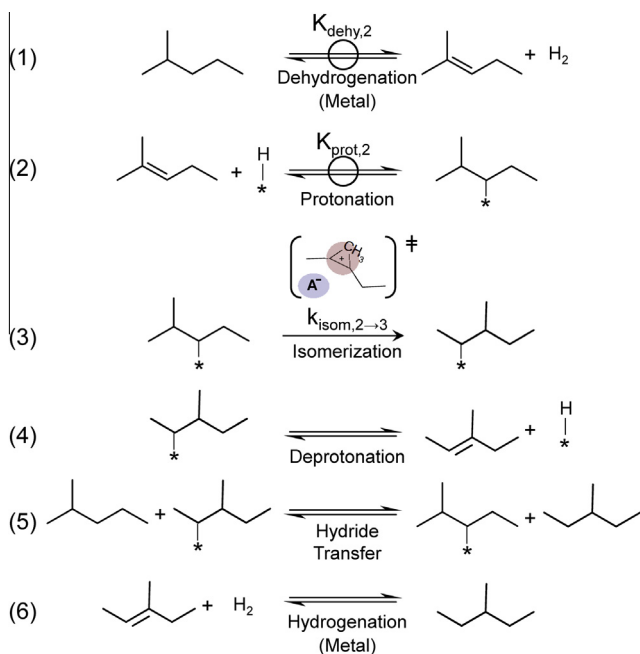
Scheme 2. Elementary steps and chemical reactions involved in 2-methylpentane isomerization on metal–acid mixtures that establish 2-methylpentane/2-methylpentene equilibrium. Chemical reactions are shown for the (de)hydrogenation on metal sites (Pt/Al$_2$O$_3$) and elementary steps for acid-catalyzed routes on H$_{8-n}$X^{n+}-W$_{12}$O$_{40}$/SiO$_2$ (X = P^{5+}, Si^{4+}, Al^{3+}, Co^{2+}). Steps 3–6 are illustrated using 3-methylpentane as the product, but analogous steps are involved in 2,3-dimethylbutane and n-hexane formation. Bonds to the Brønsted active site are denoted as "*" in molecular structures.

analyses as a lumped chemical pseudo-species, because of their rapid interconversions. These alkene (and alkoxide) pseudo-species are denoted henceforth by the superscript symbol "=" (and "*") without specifying the position of the double bond in the gaseous alkene and of the surface attachment in the alkoxides (e.g., 2-methylpentane, 2-methylpentene isomers, and 2-methylpentoxide isomers are denoted as 2MP, 2MP$^=$, and 2MP*, respectively).

The assumptions of pseudo-steady-state for alkoxides and of equilibrated hydrogenation–dehydrogenation and protonation–deprotonation steps, taken together with 2MP* and H$^+$ as the most abundant surface intermediates (MASI) and irreversible skeletal isomerization of 2MP*, lead to a rate equation for 2MP isomerization to each alkane product isomer "P" ($r_{\text{isom},2\rightarrow P}$; P = 3MP (3), 23DMB (23), or nH; full derivation in Section S.3. of Supporting Information):

$$\frac{r_{\text{isom},2\rightarrow P}}{[\text{H}^+]} = \frac{k_{\text{isom},2\rightarrow P}K_{\text{prot},2}K_{\text{dehy},2}\left(\frac{2\text{MP}}{\text{H}_2}\right)}{1 + K_{\text{prot},2}K_{\text{dehy},2}\left(\frac{2\text{MP}}{\text{H}_2}\right)} \quad (2)$$

Here, [H$^+$] is the number of accessible H$^+$ (from DTBP titration data, Section 3.1.1), $K_{\text{prot},2}$ is the equilibrium constant for 2MP$^=$ protonation to 2MP* (2-methylpent-3-oxide used as example in Scheme 2), and $k_{\text{isom},2\rightarrow P}$ is the alkoxide isomerization rate constant that forms product "P". The first and second terms in the denominator of Eq. (2) reflect the relative numbers of active sites present as unoccupied H$^+$ and 2MP*, respectively; the coverage by product-derived alkoxides is much smaller than that by 2MP*, because of the low concentrations of product alkenes at the low conversions of these experiments. All product formation rate equations have the same denominator (with terms only for H$^+$ and 2MP* species) because all products form on the same Brønsted acid sites. The

sum of rate equations similar in functional form to Eq. (2) but for each 3MP, 23DMB, and nH product gives an equation for the total 2MP isomerization rate ($r_{\text{isom},2}$) at 2MP–2MP$^=$ equilibrium:

$$\frac{r_{\text{isom},2}}{[\text{H}^+]} = \frac{k_{\text{isom},2}K_{\text{prot},2}K_{\text{dehy},2}\left(\frac{2\text{MP}}{\text{H}_2}\right)}{1 + K_{\text{prot},2}K_{\text{dehy},2}\left(\frac{2\text{MP}}{\text{H}_2}\right)} \quad (3a)$$

in terms of the sum of the individual rate constants for the isomerization to form each product

$$k_{\text{isom},2} = k_{\text{isom},2\rightarrow 3} + k_{\text{isom},2\rightarrow 23} + k_{\text{isom},2\rightarrow nH} \quad (3b)$$

$K_{\text{prot},2}K_{\text{dehy},2}$ values in Eq. (3a) are independent of the product being formed because all isomerization events originate from the same pool of equilibrated surface alkoxide species (2MP*). These equations describe the rate data shown in Fig. 2, because 2MP$^=$ concentrations remain at equilibrium with 2MP reactants at all acid sites throughout the reactor.

2MP isomerization rates that depend inversely on (H$_2$/2MP) ratios (Fig. 4b) and lie along a single curve at all H$_2$ pressures (60–90 kPa H$_2$; Fig. 4a and b) are consistent with the form of Eq. (3a) and with 2MP–2MP$^=$ equilibration:

$$\left(\frac{r_{\text{isom},2}}{[\text{H}^+]}\right)^{-1} = \frac{1}{k_{\text{isom},2}K_{\text{prot},2}K_{\text{dehy},2}}\left(\frac{\text{H}_2}{2\text{MP}}\right) + \frac{1}{k_{\text{isom},2}} \quad (4)$$

The slope and intercept of linear rate data shown in Fig. 4b, therefore, reflect the values of the kinetic and thermodynamic parameters in Eq. (4). The values of the first-order rate constant for alkene isomerization ($k_{\text{isom},2}K_{\text{prot},2}$) were regressed from the data in Fig. 4b for each POM acid to the functional form of Eq. (4) using thermodynamic data [16,31] for the gas-phase equilibrium constant for alkane–alkene equilibration ($K_{\text{dehy},2}$ = 1.10 Pa at 473 K); their values are shown in Table 2. The zero-order rate constant for alkene isomerization ($k_{\text{isom},2}$) and the equilibrium constant for the formation of alkoxide species at acid sites from gaseous alkenes ($K_{\text{prot},2}$) were regressed from the data in Fig. 4a to the functional form of Eq. (3a) using the determined $k_{\text{isom},2}K_{\text{prot},2}$ value for each POM acid. These rate data provide accurate values for $k_{\text{isom},2}K_{\text{prot},2}$, but not for $k_{\text{isom},2}$ (or $K_{\text{prot},2}$) (e.g., linear regressions of rate data measured on POM clusters give errors for $k_{\text{isom},2}K_{\text{prot},2}$ < ±0.8% of the reported values, but up to ±120% of the values reported for $k_{\text{isom},2}$). The form and mechanistic interpretation of Eq. (4) indicate that accurate $k_{\text{isom},2}$ estimates would require (H$_2$/2MP) ratios that cause detectable contributions from its intercept and, as a result, lead to kinetically detectable alkoxide coverages (the second term in the denominator of Eq. (3b)). Such small (H$_2$/2MP) ratios favor bimolecular alkene-alkoxide oligomerization reactions that can form unreactive oligomers that bind irreversibly to acid sites leading to catalyst deactivation. As a result, regressions were limited in this study to (2MP/H$_2$) ratios below ~0.1 (i.e., when the second term is much smaller than unity in the denominator of Eq. (3a)) and become less accurate at higher (2MP/H$_2$) ratios (dashed curves in Fig. 4a).

Fig. 5a shows 2MP, 3MP, 23DMB, and nH total isomerization turnover rates (normalized by H$^+$ titrated with DTBP, Table 1) as a function of (alkane/H$_2$) ratios on H$_3$PW/SiO$_2$–Pt/Al$_2$O$_3$ mixtures with 0.03 H$^+$ nm^{-2} surface density and 11.7 (Pt$_s$/H$^+$) ratios. Turnover rates increased with increasing (alkane/H$_2$) ratios for all reactants, linearly at first and then more gradually at higher reactant ratios (Fig. 4a). Isomerization turnover rates at different H$_2$ pressures lie along a single curve for each reactant (Fig. 5a and b), as expected from alkane–alkene equilibration (as in the case of 2MP reactants; Fig. 3a and b). These data show that the elementary steps in Scheme 2 accurately represent the isomerization pathways for all hexane isomers used as reactants and that all rate data can be described by:
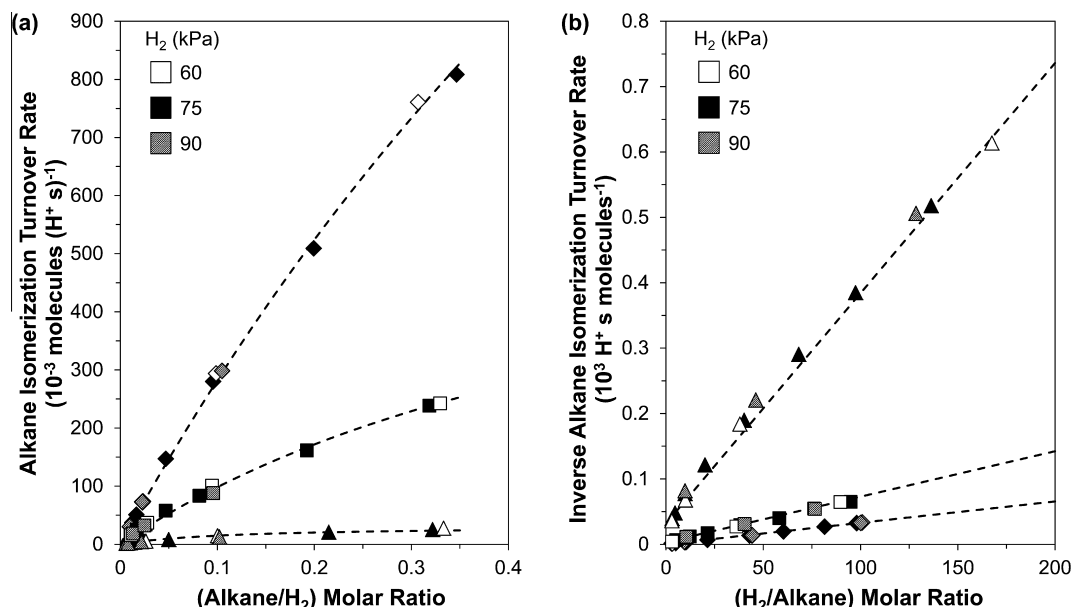
Fig. 5. (a) Isomerization turnover rates as functions of the ([R]/H_2) ratio and (b) inverse isomerization turnover rates as functions of the (H_2/[R]) ratio for (◆) 3-methylpentane, (■) 2,3-dimethylbutane, and (▲) n-hexane reactants on H_3PW/SiO_2–Pt/Al_2O_3 (Pt_S/H^+ = 11.7) (reaction conditions: 473 K, 0.5–25 kPa alkane, 60–90 kPa H_2). Dashed lines represent the regression of the data to the functional form of Eq. (5).

$$\frac{r_{isom,R}}{[H^+]} = \frac{k_{isom,R}K_{prot,R}K_{dehy,R}\left(\frac{[R]}{H_2}\right)}{1 + K_{prot,R}K_{dehy,R}\left(\frac{[R]}{H_2}\right)} \tag{5}$$

Here, $K_{dehy,R}$ is the dehydrogenation equilibrium constant for reactant "R" (R = 2MP (2), 3MP (3), 23DMB (23), or nH (nH)) calculated from tabulated thermodynamic data [31] ($K_{dehy,3}$ = 1.15 Pa, $K_{dehy,23}$ = 1.67 Pa, and $K_{dehy,nH}$ = 0.28 Pa at 473 K). $K_{prot,R}$ is the equilibrium constant for the formation of a given alkoxide regioisomer group ([R^*]) from the equilibrated alkene lump, [$R^=$], for reactant "R"; $k_{isom,R}$ is the isomerization rate constant for the total conversion of [R^*] to all isomer products. The dashed curves in Fig. 5a and b represent the regression of these data to Eq. (5) using the method described above for 2MP reactants to obtain $k_{isom,R}K_{prot,R}$, $K_{prot,R}$, and $K_{dehy,R}$ values. As in the case of 2MP reactants, $k_{isom,R}$-$K_{prot,R}$ values for 3MP, 23DMB, and nH reactants can be determined more accurately than $k_{isom,R}$ values (or $K_{prot,R}$) (e.g., linear regressions of data in Fig. 5b give errors for $k_{isom,R}K_{prot,R}$ < ±0.9% of the reported values, but errors for $k_{isom,R}$ up to ±430% of the reported values). The $k_{isom,R}K_{prot,R}$ values for 3MP, 23DMB, and nH reactants on POM/SiO_2–Pt/Al_2O_3 mixtures with Si, Al, and Co central atoms were obtained by regression of rate data to the functional form of Eq. (5) at low (alkane/H_2) ratios (75 kPa H_2, <1.9 kPa alkane).

A rigorous analysis of the effects of acid strength on isomerization rate constants and selectivities requires that we dissect $k_{isom,R}$-$K_{prot,R}$ values into those for the formation of each *individual* isomer product ($k_{isom,R\rightarrow P}K_{prot,R}$). The data and discussion in Section 3.1.2 showed that measured alkane isomerization selectivities vary with reactant alkane pressure and do not reflect the selectivity for the formation of *primary* isomers (defined as those formed from reactant alkenes in one sojourn at an acid site); therefore, these selectivities cannot be used to calculate the individual formation rate for each isomer and to determine, in this manner, the $k_{isom,R\rightarrow P}$-$K_{prot,R}$ values. This constraint precludes the determination of each $k_{isom,R\rightarrow P}K_{prot,R}$ value for most *individual* isomer products formed from each reactant (except approximately when one isomer predominates among products). As we show next, however, $k_{isom,2\rightarrow3}$-$K_{prot,2}$ values, and consequently 2MP isomerization selectivities to 3MP and the ratio of those selectivities to those for isomerization

products that vary backbone length, can be determined explicitly, without the use of measured product selectivities, from the measured lumped $k_{isom,R}K_{prot,R}$ values for each isomer reactant.

The functional form of Eq. (3b) for each reactant allows one to expand $k_{isom,R}K_{prot,R}$ values for each reactant "R" in terms of $k_{isom,R\rightarrow P}K_{prot,R}$ values for each product "P" formed from reactant "R" (noting that 22DMB formation is excluded from 23DMB conversion rates):

$$k_{isom,2}K_{prot,2} = k_{isom,2\rightarrow3}K_{prot,2} + k_{isom,2\rightarrow23}K_{prot,2} + k_{isom,2\rightarrow nH}K_{prot,2} \tag{6a}$$

$$k_{isom,3}K_{prot,3} = k_{isom,3\rightarrow2}K_{prot,3} + k_{isom,3\rightarrow23}K_{prot,3} + k_{isom,3\rightarrow nH}K_{prot,3} \tag{6b}$$

$$k_{isom,23}K_{prot,23} = k_{isom,23\rightarrow2}K_{prot,23} + k_{isom,23\rightarrow3}K_{prot,23} \tag{6c}$$

$$k_{isom,nH}K_{prot,nH} = k_{isom,nH\rightarrow2}K_{prot,nH} + k_{isom,nH\rightarrow3}K_{prot,nH} \tag{6d}$$

These forward and reverse isomerization rate constants ($k_{isom,2\rightarrow23}$-$K_{prot,2}$ and $k_{isom,23\rightarrow2}K_{prot,23}$ for example) are measured at reaction conditions where unoccupied H^+ sites are the *single* most abundant surface species and alkoxide isomerization is the *single* kinetically-relevant step. In such cases, forward and reverse isomerization events are mediated by the same kinetically-relevant transition state and must obey the principle of microscopic reversibility even when the isomerization reactions are far from equilibrium [31]. The ratio of the rate constants that describe such reactions is given by the equilibrium constant ($K_{ene,R\leftrightarrow P}$) for the overall reaction (i.e., formation of the equilibrated [$P^=$] lump for product "P" from the equilibrated [$R^=$] lump for reactant "R"), which may be calculated from tabulated gas-phase thermodynamic data at the given reaction temperature (473 K):

$$K_{ene,2\leftrightarrow3} = \frac{k_{isom,2\rightarrow3}K_{prot,2}}{k_{isom,3\rightarrow2}K_{prot,3}} \tag{7a}$$

$$K_{ene,2\leftrightarrow23} = \frac{k_{isom,2\rightarrow23}K_{prot,2}}{k_{isom,23\rightarrow2}K_{prot,23}} \tag{7b}$$

$$K_{\text{ene},2\to\text{nH}} = \frac{k_{\text{isom},2\to\text{nH}}K_{\text{prot},2}}{k_{\text{isom},\text{nH}\to2}K_{\text{prot},\text{nH}}} \tag{7c}$$

$$K_{\text{ene},23\to3} = \frac{k_{\text{isom},23\to3}K_{\text{prot},23}}{k_{\text{isom},3\to23}K_{\text{prot},3}} \tag{7d}$$

$$K_{\text{ene},\text{nH}\leftrightarrow3} = \frac{k_{\text{isom},\text{nH}\to3}K_{\text{prot},\text{nH}}}{k_{\text{isom},3\to\text{nH}}K_{\text{prot},3}} \tag{7e}$$

These relations can be used to simplify Eqs. (6a)–(6d) to:

$$k_{\text{isom},2\to3}K_{\text{prot},2} = k_{\text{isom},2}K_{\text{prot},2} - k_{\text{isom},2\to23}K_{\text{prot},2}$$
$$- k_{\text{isom},2\to\text{nH}}K_{\text{prot},2} \tag{8a}$$

$$k_{\text{isom},2\to3}K_{\text{prot},2} = k_{\text{isom},3}K_{\text{prot},3}K_{\text{ene},2\leftrightarrow3}$$
$$- k_{\text{isom},3\to23}K_{\text{prot},3}K_{\text{ene},2\leftrightarrow3}$$
$$- k_{\text{isom},3\to\text{nH}}K_{\text{prot},3}K_{\text{ene},2\leftrightarrow3} \tag{8b}$$

$$0 = -k_{\text{isom},23}K_{\text{prot},23}K_{\text{ene},2\leftrightarrow23} + k_{\text{isom},2\to23}K_{\text{prot},2}$$
$$+ k_{\text{isom},3\to23}K_{\text{prot},3}K_{\text{ene},2\leftrightarrow3} \tag{8c}$$

$$0 = -k_{\text{isom},\text{nH}}K_{\text{prot},\text{nH}}K_{\text{ene},2\leftrightarrow\text{nH}} + k_{\text{isom},2\to\text{nH}}K_{\text{prot},2}$$
$$+ k_{\text{isom},3\to\text{nH}}K_{\text{prot},3}K_{\text{ene},2\leftrightarrow3} \tag{8d}$$

Adding Eqs. (8a)–(8d), gives an explicit expression for $k_{\text{isom},2\to3}K_{\text{prot},3}$ in terms of the measurable $k_{\text{isom},R}K_{\text{prot},R}$ and $K_{\text{ene},2\leftrightarrow R}$ values for each reactant:

$$k_{\text{isom},2\to3}K_{\text{prot},2} = \frac{1}{2}\big(k_{\text{isom},2}K_{\text{prot},2} + k_{\text{isom},3}K_{\text{prot},3}K_{\text{ene},2\leftrightarrow3}$$
$$- k_{\text{isom},23}K_{\text{prot},23}K_{\text{ene},2\leftrightarrow23} - k_{\text{isom},\text{nH}}K_{\text{prot},\text{nH}}K_{\text{ene},2\leftrightarrow\text{nH}}\big) \tag{9}$$

The selectivity to methyl-shift isomerization events relative to those events that vary backbone length (s_{MS}) can then be calculated from $k_{\text{isom},2}K_{\text{prot},2}$ and $k_{\text{isom},2\to3}K_{\text{prot},2}$ values:

$$s_{\text{MS}} = \frac{r_{\text{isom},2\to3}}{r_{\text{isom},2\to23} + r_{\text{isom},2\to\text{nH}}} = \frac{k_{\text{isom},2\to3}K_{\text{prot},2}}{k_{\text{isom},2}K_{\text{prot},2} - k_{\text{isom},2\to3}K_{\text{prot},2}} \tag{10}$$

Here, $r_{\text{isom},2\to3}$, $r_{\text{isom},2\to23}$, and $r_{\text{isom},2\to\text{nH}}$ are, respectively, rates of methyl shift, branching, and chain lengthening isomerization events from 2MP⁼.

We conclude that first-order alkene isomerization rate constants measured on POM/SiO₂–Pt/Al₂O₃ mixtures ($k_{\text{isom},R}K_{\text{prot},R}$; Fig. 6a) reflect the reactivity of gaseous [R⁼] species in equilibrium with the reactant alkane at H⁺. From this mechanistic analysis, we can determine $k_{\text{isom},2\to3}K_{\text{prot},2}$ values and selectivities for 3MP formation from 2MP explicitly and also the ratio of methyl shift events to those that lengthen or shorten the backbone (s_{MS}) without the use of measured isomerization selectivities that reflect, in part, transport restrictions of product alkenes within acid domains instead of the rate constants for the formation of *individual* products from measured $k_{\text{isom},R}K_{\text{prot},R}$ values for each reactant. Values of $k_{\text{isom},2\to3}K_{\text{prot},2}$ reflect the free energy barrier for forming the transition state that mediates 2MP and 3MP interconversion from gaseous 2MP⁼; these values are used in Section 3.3 to assess the effects of acid strength on the stability of such transition states. Values of s_{MS} indicate the tendency for 2MP reactants to methyl shift rather than branch or chain lengthen, thus providing a measure of isomerization product selectivities that is free of transport corruptions. In Section 3.4, s_{MS} values determined for POM/SiO₂–Pt/Al₂O₃ mixtures with P, Si, Al, and Co central atoms are used to probe the effects of acid strength on isomerization selectivities.

3.2. Mechanistic assessment of the effects of acid strength on isomerization rates

Fig. 6a shows $k_{\text{isom},R}K_{\text{prot},R}$ values (in a logarithmic scale) for 2MP, 3MP, 23DMB, and nH reactants on POM/SiO₂–Pt/Al₂O₃ mixtures as a function of DPE values previously reported for POM clusters with P, Si, Al, and Co central atoms [3]. The $k_{\text{isom},R}K_{\text{prot},R}$ value for each hexane isomer reactant decreases exponentially with increasing DPE. POM clusters with fewer protons (and higher-valent central atoms) have more stable conjugate anions and thus smaller DPE values, because the partial charge in protons leads to lower electron density for clusters with fewer protons and, consequently, higher electron affinity. The exponential effects of DPE on rate constants predominantly reflect concomitant effects on activa-
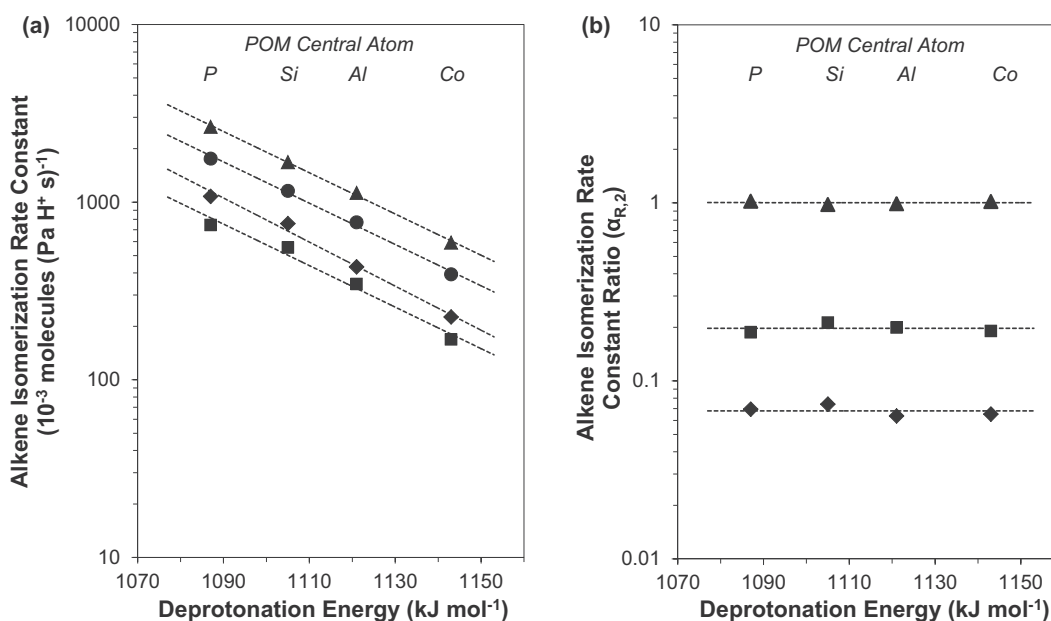
Fig. 6. (a) Alkene isomerization rate constants ($k_{\text{isom},R}K_{\text{prot},R}$) for (●) 2-methylpentane, (▲) 3-methylpentane, (■) 2,3-dimethylbutane, and (◆) n-hexane reactants and (b) $k_{\text{isom},R}K_{\text{prot},R}K_{\text{ene},2\leftrightarrow R}/k_{\text{isom},2}K_{\text{prot},2}$ ratios for (▲) 3-methylpentane, (■) 2,3-dimethylbutane, and (◆) n-hexane reactants as functions of deprotonation energy for $H_{8-n}X^{n+}W_{12}O_{40}$ (X = P, Si, Al, Co) (473 K). The dashed lines in (a) are exponential fits of the data to deprotonation energies for Keggin clusters and in (b) are the averages of the data for each ratio.

tion energies, instead of activation entropies [3,8] because isomerization TS structures are similar on POM clusters with different central atom [8]. When DPE predominantly influences activation energies, the effects of DPE on $k_{isom,R}K_{prot,R}$ can be expressed in terms of derivatives as:

$$
\begin{aligned}
\frac{d(\ln(k_{isom,R}K_{prot,R}))}{d(DPE)} &= \frac{1}{k_{isom,R}K_{prot,R}}\frac{d(k_{isom,R}K_{prot,R})}{d(DPE)} \\
&= -\frac{1}{RT}\frac{d(E_{A,R})}{d(DPE)}
\end{aligned}
\tag{11}
$$

Here, $E_{A,R}$ is the measured activation barrier for reactant "R". The linear dependence of $\ln(k_{isom,R}K_{prot,R})$ on DPE (Fig. 6a) indicates that $d(E_{A,R})/d(DPE)$ values for all hexane isomer reactants are essentially independent of DPE on these POM clusters. The small values of the slopes of the dashed lines in Fig. 6a ($d(\ln(k_{isom,R}K_{prot,R}))/d(DPE) = -0.03$ mol kJ^{-1} for all reactants) and the functional form of Eq. (11) indicate that the measured activation energies vary in magnitude much less than the concomitant changes in DPE. Measured activation energies for all hexane isomer reactants were similarly sensitive to changes in DPE ($d(E_{A,R})/d(DPE) = 0.11$), for which $k_{isom,R}K_{prot,R}$ rate constants vary by about a factor of 4 for each POM composition. Similar sensitivities of $k_{isom,R}K_{prot,R}$ rate constants to changes in DPE for these different isomer reactants that form different sets of isomer products provides qualitative evidence that all isomerization events are similarly dependent on DPE.

Isomerization leads to multiple products and $k_{isom,R}K_{prot,R}$ is a lumped rate constant reflecting the total rate of isomerization of the gaseous equilibrated alkene lump for reactant "R" to each individual product "P" with rate constant $k_{isom,R\to P}K_{prot,R}$ (Eqs. (6a)–(6d)). Therefore, the effects of DPE on $k_{isom,R}K_{prot,R}$ are given by the summation of those on $k_{isom,R\to P}K_{prot,R}$ rate constants for each product "P" of reactant "R":

$$
\frac{d(k_{isom,R}K_{prot,R})}{d(DPE)} = \sum_P \frac{d(k_{isom,R\to P}K_{prot,R})}{d(DPE)}
\tag{12}
$$

Eq. (11) and equations analogous to Eq. (11) that describe the effects of DPE on each $k_{isom,R\to P}K_{prot,R}$ rate constant may be solved implicitly for each of the derivatives in Eq. (12). Filling these solutions into Eq. (12) shows that measured $d(E_{A,R})/d(DPE)$ values are given by the rate-average (or selectivity-average) of those for each isomer product that a reactant forms:

$$
\frac{d(E_{A,R})}{d(DPE)} = \frac{\sum_P k_{isom,R\to P}K_{prot,R}\frac{d(E_{A,R\to P})}{d(DPE)}}{k_{isom,R}K_{prot,R}} = \sum_P S_{R\to P}\frac{d(E_{A,R\to P})}{d(DPE)}
\tag{13}
$$

Here, $E_{A,R\to P}$ is the activation barrier to form the TS that gives the isomer product "P" from reactant "R" and $S_{R\to P}$ is the selectivity to isomer product "P" from reactant "R". According to Eq. (13), $d(E_{A,R})/d(DPE)$ values that are similar for each reactant and essentially independent of DPE require the stability of all isomerization TS to be similarly sensitive to DPE (with $(E_{A,R\to P})/d(DPE) = 0.11$ for all kinetically-relevant isomerization steps). Such similar sensitivities would lead, in turn, to isomerization selectivities ($S_{R\to P}$) that cannot depend on DPE (and acid strength) for these POM clusters.

The relative stabilities of the ensembles of TS structures that mediate the isomerizations between 2MP, 3MP, 23DMB, and nH reactants cannot be compared directly from their $E_{A,R}$ values because these activation energies are referenced to different reactants. The gaseous alkene reactant lumps ([R$^=$]) have different gas-phase stabilities related to the equilibrium constant for the formation of the given equilibrated [R$^=$] lump from a common reference equilibrated lump. In the context of transition state theory, $k_{isom,R\to P}K_{prot,R}$ values reflect free energy barriers ($\Delta G_{R\to P}^{\ddagger}$) given by the difference between the free energies for the TS that mediates

the conversion of "R" to "P" (or "P" to "R", $G_{P\leftrightarrow R}^{\ddagger}$) and for the gaseous alkene reactant lump ($G_{ene,R}$):

$$
\Delta G_{R\to P}^{\ddagger} = G_{R\to P}^{\ddagger} - G_{ene,R} = -RT\ln\left(\frac{h}{k_BT}k_{isom,R\to P}K_{prot,R}\right)
\tag{14}
$$

Here, k_B and h are the Boltzmann and Planck constants, respectively. Free energy barriers calculated in this manner using $k_{isom,R}K_{prot,R}$ rate constants ($\Delta G_R^{\ddagger}$) can be related to those for each product formed using the functional form of Eq. (3b) for the given reactant "R" and Eq. (14) (shown in Scheme 3 for 2MP, 3MP, and 23DMB reactants):

$$
\begin{aligned}
\Delta G_R^{\ddagger} &= -RT\ln\left(\sum_P \exp\left(\frac{-\left(G_{R\to P}^{\ddagger} - G_{ene,R}\right)}{RT}\right)\right) \\
&= -RT\ln\left(\frac{h}{k_BT}k_{isom,R}K_{prot,R}\right)
\end{aligned}
\tag{15}
$$

Here, $\Delta G_R^{\ddagger}$ accounts for the additive contributions of all TS to measured $k_{isom,R}K_{prot,R}$ values. The free energy difference between the gaseous alkene lump ([R$^=$]) species and the gaseous 2MP$^=$ ($\Delta G_{ene,2\leftrightarrow R}$) can be added to both sides of Eq. (15) to make all TS energies relative to the same reference state (gaseous 2MP$^=$):

$$
\Delta G_R^{\ddagger\prime} = \Delta G_R^{\ddagger} + \Delta G_{ene,2\leftrightarrow R} = -RT\ln\left(\sum_P \exp\left(\frac{-(G_{R\to P}^{\ddagger} - G_{ene,2})}{RT}\right)\right)
\tag{16}
$$

In this case, $\Delta G_R^{\ddagger\prime}$ is the free energy barrier for the ensemble of TS accessible to reactant "R" referenced to gaseous 2MP$^=$ (shown in Scheme 3 for 2MP$^=$, 3MP$^=$ and 23DMB$^=$ reactants) and $G_{ene,2}$ is the free energy for the gaseous 2MP$^=$. We can then compare $\Delta G_R^{\ddagger\prime}$ values for each reactant to those for 2MP by taking the ratio of the isomerization rate constant for each reactant isomer ($k_{isom,R}K_{prot,R}$) (normalized by the equilibrium constant for forming the gaseous reactant alkene lump [R$^=$] from gaseous 2MP$^=$ ($K_{ene,2\leftrightarrow R}$)) to the isomerization rate constant for 2MP ($k_{isom,2}K_{prot,2}$):

$$
\alpha_{R,2} = \frac{k_{isom,R}K_{prot,R}K_{ene,2\leftrightarrow R}}{k_{isom,2}K_{prot,2}} = \exp\left(\frac{-(\Delta G_R^{\ddagger\prime} - \Delta G_2^{\ddagger})}{RT}\right)
\tag{17}
$$

The value of $\alpha_{R,2}$ reflects the free energy difference between that for the isomerization TS structures accessible to reactant "R" and that for the TS structures accessible to 2MP$^=$, thus providing a rigorous assessment of the relative stability of the two ensembles of transition states ($\Delta G_R^{\ddagger\prime} - \Delta G_2^{\ddagger}$). The $\alpha_{R,2}$ values determined for 3MP, 23DMB, and nH reactants are essentially independent of DPE on W-POM acids with different central atoms (Fig. 6b) because $k_{isom,R}K_{prot,R}$ values for each alkane reactant depend similarly on acid strength. Values of $\alpha_{R,2}$ are near unity for 3MP because 2MP and 3MP predominantly form each other during their respective isomerization reactions via the same transition state. The $\alpha_{R,2}$ values for 23DMB and nH reactants are much smaller than unity (0.20 ± 0.02 and 0.068 ± 0.008 for 23DMB and nH, respectively) because the transition states for chain lengthening and shortening (the predominant isomerization events for 23DMB and nH reactants, respectively) are less stable than those that mediate methyl shifts (the predominant isomerization event for 2MP reactants). Eq. (17) gives free energy barrier differences that indicate free energy barriers are 6.3 ± 0.4 kJ mol^{-1} and 10.5 ± 0.4 kJ mol^{-1} lower for 2MP isomerization than for 23DMB and nH isomerization, respectively.

3.3. Mechanistic assessment of the effects of acid strength on isomerization transition state energies

The following discussion assesses calculated $k_{isom,2\to3}K_{prot,2}$ values (Eq. (9)) mechanistically, then further analyzes their values in
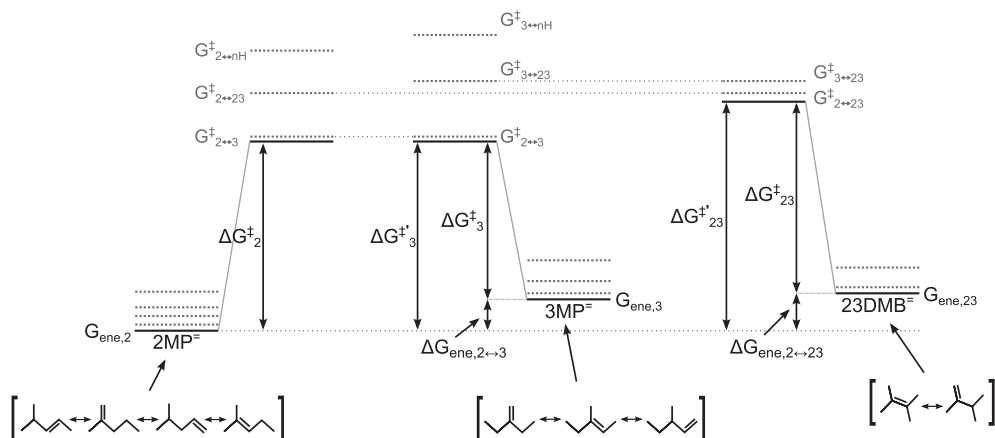
Scheme 3. Reaction coordinate diagram depicting the free energies of 2MP$^=$ ($G_{ene,2}$), 3MP$^=$ ($G_{ene,3}$), and 23DMB$^=$ ($G_{ene,23}$) regioisomer groups and the free energies of the isomerization transition states accessible to each of these groups (2MP$^=$: $G^\ddagger_{2\leftrightarrow3}$, $G^\ddagger_{2\leftrightarrow23}$, and $G^\ddagger_{2\leftrightarrow nH}$; 3MP$^=$: $G^\ddagger_{2\leftrightarrow3}$, $G^\ddagger_{3\leftrightarrow23}$ and $G^\ddagger_{3\leftrightarrow nH}$; 23DMB$^=$: $G^\ddagger_{2\leftrightarrow23}$ and $G^\ddagger_{3\leftrightarrow23}$). Free energy barriers for $k_{isom,2}K_{prot,2}$ ($\Delta G^\ddagger_2$), $k_{isom,3}K_{prot,3}$ ($\Delta G^\ddagger_3$), $k_{isom,23}K_{prot,23}$ ($\Delta G^\ddagger_{23}$), $k_{isom,3}K_{prot,3}K_{ene,2\leftrightarrow3}$ ($\Delta G^{\ddagger\prime}_3$), and $k_{isom,23}K_{prot,23}K_{ene,2\leftrightarrow23}$ ($\Delta G^{\ddagger\prime}_{23}$) and free energy differences for $K_{ene,2\leftrightarrow3}$ ($\Delta G_{ene,2\leftrightarrow3}$) and $K_{ene,2\leftrightarrow23}$ ($\Delta G_{ene,2\leftrightarrow23}$) are also shown.

more detail using thermochemical cycles. In doing so, we seek to probe how specific catalyst properties determine the stability of *individual* isomerization transition states and what causes the significant attenuation of DPE effects on activation barriers for such transition states. Fig. 7 shows values of $k_{isom,2\to3}K_{prot,2}$, calculated from $k_{isom}K_{prot,R}$ values using the functional form of Eq. (9), for 2MP, 3MP, 23DMB, and nH reactant on POM clusters with P, Si, Al, and Co central atoms as a function of their DPE. The slope of the dashed line for the $k_{isom,2\to3}K_{prot,2}$ data in Fig. 7 ($d(\ln(k_{isom,2\to3}K_{prot,2}))/d(DPE) = -0.03$ mol kJ^{-1}) is much smaller than unity, indicating, according to an equation analogous to Eq. (11) describing the effects of DPE on $k_{isom,2\to3}K_{prot,2}$, that activation barriers for methyl shift isomerization transition states differ in energy among catalysts much less than their concomitant changes in DPE ($d(E_{A,2\to3})/d(DPE) = 0.11 < 1$). Scheme 4 shows the reaction coordinate for 2MP$^=$ (shown as 2-methylpent-2-ene as the example) conversion to 3MP$^=$ and the energies that determine the activation barrier reflected in its lumped kinetic parameter ($k_{isom,2\to3}K_{prot,2}$). Activation energies for $k_{isom,2\to3}K_{prot,2}$ include the energies to protonate the lumped gaseous 2MP$^=$ species by reaction with protons at POM Brønsted acid sites (E_{prot} in Scheme 4) and to rearrange 2MP* species to form the transition state that mediates methyl shifts for the equilibrated mixtures of adsorbed alkoxides ($E_{isom,3MP}$ in Scheme 4). Thermochemical cycles are used next to dissect these methyl shift activation energies into those for a sequence of hypothetical steps, for which experiments or calculations can provide accurate energies, using a formalism previously applied to alkanol dehydration [3,7] and n-hexane isomerization [8] reactions on solid acids.

A thermochemical cycle that converts gaseous 2MP$^=$ species into the methyl shift transition state (Scheme 4) involves deprotonation (DPE) of the POM clusters by overcoming interactions of H$^+$ with conjugate anion, formation of gaseous cycloalkyl carbenium ions resembling the TS cation (structure resembles Scheme 5(A) for 2MP–3MP interconversion) by reactions of gaseous H$^+$ and 2MP$^=$ ($E_{gas,2\to3}$), and the interaction energy between the gaseous TS cations and the conjugate anion of the POM solid acid at the TS ($E_{int,2\to3}$):

$$E_{A,2\to3} = DPE + E_{gas,2\to3} + E_{int,2\to3} \qquad (18)$$

Here, DPE and $E_{int,2\to3}$ reflect ion-pair interactions of H$^+$ and the TS cation, respectively, with the same POM anion. Such interactions typically involve an ionic component reflecting classical electrostatic interactions between ions, when they approach each
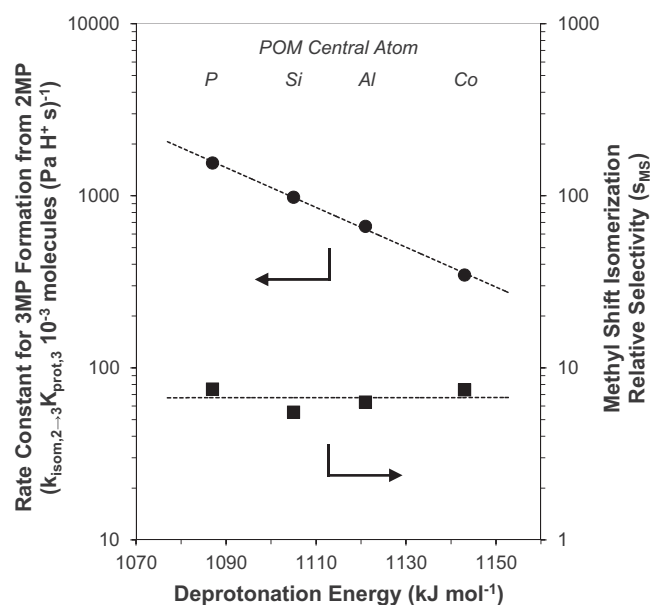
Fig. 7. Rate constants for 2-methylpentene isomerization to 3-methylpentene ($k_{isom,2\to3}K_{prot,2}$, ●) and selectivities for methyl shift isomerization events relative to isomerization events that vary backbone length (s_{MS}, ■) at 473 K as a function of deprotonation energy for H$_{8-n}$X^{n+}W$_{12}$O$_{40}$ (X = P, Si, Al, Co). The dashed lines are an exponential fit of $k_{isom,2\to3}K_{prot,2}$ values to deprotonation energies and the average of s_{MS} values for Keggin clusters.

other, and a covalent component reflecting structural and electronic relaxation induced by ions in close proximity with each other [9]. The $E_{gas,2\to3}$ value is the energy required to form the gaseous analog of the relevant cycloalkyl carbenium ion transition state ([C$_6$H$^\ddagger_{13}$]$^+_{(g)}$) from gaseous 2MP$^=$ and a free gaseous H$^+$:

$$2MP^=_{(g)} + H^+_{(g)} \to [C_6H^\ddagger_{13}]^+_{(g)} \qquad (19)$$

The sensitivity of each energy term in the thermochemical cycle (Eq. (18)) to DPE ultimately accounts for the observed effects of DPE on $k_{isom,2\to3}K_{prot,2}$ values (Fig. 7):

$$\frac{d(E_{A,2\to3})}{d(DPE)} = 1 + \frac{d(E_{int,2\to3})}{d(DPE)} \qquad (20)$$

The term for $d(E_{gas,2\to3})/d(DPE)$ is absent in Eq. (20) (even though it appears in Eq. (18)), because $E_{gas,2\to3}$ is a property of the gaseous
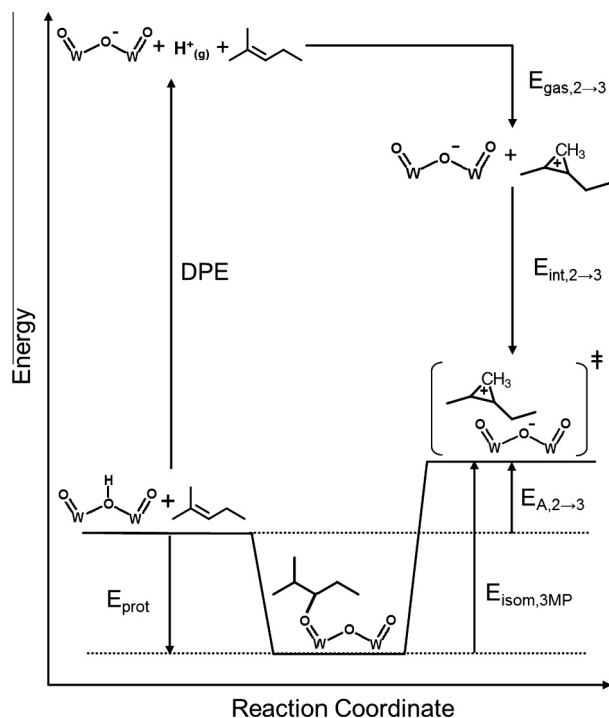
Scheme 4. Thermochemical cycle accounting for activation energies of Brønsted acid-catalyzed isomerization reactions (shown for 3MP products). Activation energies of $k_{isom,2\to3}K_{prot,2}$ ($E_{A,2\to3}$) are the sum of the intrinsic isomerization activation energies ($E_{isom,3MP}$) and 2-methylpentene protonation energies at the acid site (E_{prot}). $E_{A,2\to3}$ values depend on catalyst deprotonation energies (DPE), gas-phase protonation of the alkene to form the gaseous analog of the transition state ($E_{gas,2\to3}$), and transition state interaction energies ($E_{int,2\to3}$).
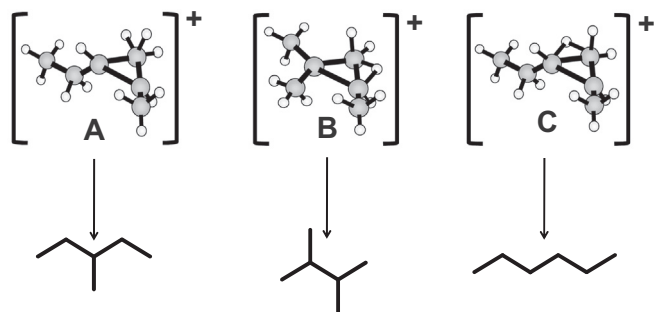
Scheme 5. Proposed cyclopropyl carbenium ions at isomerization transition states forming (A) 3-methylpentane, (B) 2,3-dimethylbutane, and (C) n-hexane [27]. 3-Methylpentane transition states involve cleavage and formation of C–C bonds to shift the methyl group along the hydrocarbon backbone. 2,3-Dimethylbutane and n-hexane transition states involve concerted cleavage and formation of C–C and C–H bonds to rearrange the hydrocarbon backbone.

species (Eq. (19)) and thus unaffected by the identity or DPE of the acid catalyst. Activation energies of methyl shift isomerizations ($E_{A,2\to3}$) increase less than the commensurate changes in DPE because interactions between the conjugate anion and cationic moieties at TS recover a large fraction of the additional energy needed to deprotonate weaker acids, as also shown previously for acid-catalyzed reactions that are mediated by ion-pair transition states [3,7]. Thus, weaker acids have larger DPE values and more negative values of $E_{int,2\to3}$ that offset each other in activation energies.

Mechanistic assessments of rate constants for the formation of other *individual* isomerization products from 2MP$^=$ or any of the other alkenes ($k_{isom,R\to P}K_{prot,R}$) lead to similar thermochemical

cycles and consequently to equations similar to that for $k_{isom,2\to3}K_{prot,2}$ (Eq. (20)). The replacement of the $d(E_{A,R\to P})/d(DPE)$ term in Eq. (13) with equations analogous to Eq. (20) for each hexane isomer shows that the attenuation of the effects of DPE on the activation barriers ($d(E_{A,R})/d(DPE) < 1$) for $k_{isom,R}K_{prot,R}$ rate constants ($E_{A,R}$) reflect the selectivity average of those for $k_{isom,R\to P}K_{prot,R}$ for each reactant

$$\frac{d(E_{A,R})}{d(DPE)} = 1 + \sum_P \frac{k_{isom,R\to P}K_{prot,R}}{k_{isom,R}K_{prot,R}} \frac{d(E_{int,R\to P})}{d(DPE)} = 1 + \sum_P S_{R\to P} \frac{d(E_{int,R\to P})}{d(DPE)}$$ (21)

Here, $E_{int,R\to P}$ values reflect the ionic and covalent interactions between the conjugate anion and the TS that is kinetically-relevant for the conversion of each reactant "R" to each product "P" and $S_{R\to P}$ is the selectivity to isomer product "P" from reactant "R". The linear dependence of $\ln(k_{isom,R}K_{prot,R})$ on DPE (Fig. 6a) indicates, according to the functional form of Eq. (11), that $d(E_{A,R})/d(DPE)$ values and, in turn, the right side of Eq. (21) is similar for all hexane isomer reactants and essentially independent of DPE on these POM clusters. These results suggests that $E_{int,R\to P}$ values for all the transitions states that interconvert all hexene isomers depend similarly on DPE (with $d(E_{int,R\to P})/d(DPE) = -0.89$ for every one of the isomerization reactions); consequently, isomerization selectivities ($S_{R\to P}$) are independent of DPE on these POM clusters. The factors responsible for such similar DPE effects on selectivities are discussed in the next section.

3.4. Mechanistic assessment of the effects of acid strength on isomerization selectivities

In this section, calculated s_{MS} values for 2MP reactants (Eq. (10)) are assessed mechanistically, and then analyzed in more detail using the thermochemical cycles of Section 3.3. Fig. 7 shows measured s_{MS} values for 2MP reactants on POM/SiO$_2$–Pt/Al$_2$O$_3$ mixtures (P, Si, Al, Co central atoms) as a function of their DPE values. Values of s_{MS} were greater than unity and essentially independent of DPE on these POM clusters, having a mean value of 6.7 ± 1.5 (95% confidence interval). Such s_{MS} values greater than unity suggest that the cycloalkyl carbenium ion transition states that form 23DMB and nH from 2MP reactants (Scheme 5(B) and (C), respectively) are less stable than those that form 3MP from 2MP reactants (Scheme 5(A)), consistent with lower DFT-derived activation barriers for reactions on an aluminosilicate site that form 3-methyl-2-pentene from 2-methylpent-2-ene (71 kJ/mol) [27] than those forming 2,3-dimethyl-2-butene from 2-methylpent-2-ene (117 kJ/mol) [27].

The significant role of $E_{gas,R\to P}$ in determining the magnitude of activation energies (Eq. (18)), but not their dependence on DPE (Eq. (20)), indicates that reactions that are more demanding (i.e., have larger activation energies) do not necessarily sense acid strength more strongly (i.e., exhibit a larger slope with DPE). The effects of acid strength on isomerization selectivities reflect only the relative ability of these cationic transition states to recover differences in DPE among acids through concomitant changes in their interaction energies with the conjugate anions of these acids. "Proton-like" transition states with localized positive charges that can closely approach the anion interact more strongly with the anion, which leads to weaker DPE effects on their activation energies than that of larger transition states with more diffuse positive charges.

When pre-exponential factors are essentially independent of DPE (Section 3.2), the effects of DPE on s_{MS} values are given by:

$$\frac{d(\ln(s_{MS}))}{d(DPE)} = -\frac{1}{RT}\left(\frac{d(E_{int,2\to3})}{d(DPE)} - \frac{d(E_{int,2\to23+nH})}{d(DPE)}\right)$$ (22)

because DPE effects on isomerization activation barriers depend only on the concomitant effects on transition state interaction ener-

gies (Eq. (17)). Here, $E_{int,2\to23+nH}$ is the rate-averaged interaction energy for the transition states that mediate nH and 23DMB formation from 2MP defined by:

$$E_{int,2\to23+nH} = \frac{k_{isom,2\to23}}{k_{isom,2\to23} + k_{isom,2\to nH}} E_{int,2\to23}$$
$$+ \frac{k_{isom,2\to nH}}{k_{isom,2\to23} + k_{isom,2\to nH}} E_{int,2\to nH} \quad (23)$$

The s_{MS} values are essentially independent of DPE (Fig. 7), indicating that interaction energies are similarly sensitive to changes in DPE for the transition states that mediate methyl shift, branching, and chain lengthening isomerizations events $(d(E_{int,2\to3})/d(DPE) = d(E_{int,2\to23+nH})/d(DPE) = -0.89$ in Eq. (22)). The similar amount and location of cationic charge at these TS causes them to recover a similar fraction of the DPE changes among these clusters. In such cases, the specific kinetic hurdles for a given isomerization event (reflected in the magnitude of $E_{gas,R\to P}$ for that reaction in Eq. (18)) does not influence how this activation barrier varies with acid strength.

This mechanistic analysis shows that s_{MS} values rigorously reflect the differences in free energy barriers between TS that shift the methyl group and those that vary backbone length of 2MP reactants, and, as a result, provide a probe of *primary* product selectivities (defined as those formed from reactant alkenes in one surface sojourn) free of transport artifacts. The value of s_{MS}, or the tendency of alkenes with 2MP backbones to form alkenes with 3MP, nH, or 23DMB backbones, is unaffected by the DPE, and thus the acid strength, of POM clusters because of the similar amount and localization of cationic charge at all isomerization TS. In such cases, acid strength alone cannot be used to improve the selective isomerization to any one of these hexane isomers from a given reactant, nor can it be used for any other conversion where TS cations in competing pathways have similar charge amount and localization.

4. Conclusions

The effects of acid strength on reactivity and selectivity are demonstrated using 2-methylpentane (2MP), 3-methylpentane (3MP), 2,3-dimethylbutane (23DMB), and n-hexane (nH) isomerization routes on well-defined solid Brønsted acids in mixtures with Pt/Al$_2$O$_3$ cocatalysts. Fast dehydrogenation–hydrogenation reactions at Pt sites equilibrate alkanes and all alkene isomers of a given backbone structure at these sites providing a low and constant concentration of alkenes that disfavor oligomerization reactions at acid sites that can lead to catalyst deactivation. Alkenes isomerize to one another through alkoxide backbone rearrangements at acid sites via similar elementary steps and with similar rate expressions. Alkene isomerization rate constants for each hexane isomer ($k_{isom,R}K_{prot,R}$) were measured on Keggin polyoxometalate (POM) clusters using mechanism-based interpretations of rate data and titrations that count the number of reactive H$^+$. These rate constants reflect the stabilities of cycloalkyl carbenium ion transition states, which mediate kinetically-relevant alkoxide isomerization steps, relative to an equilibrated lump of gaseous reactant alkenes and unoccupied sites; rate constants decrease exponentially with increasing deprotonation energies (DPE) on Keggin POM for all reactants because ion-pair transition states contain less stable conjugate anions on weaker acids. Such transition states attenuate changes in DPE on activation barriers because interactions between the conjugate anion and cationic moieties at these transition states recover most of the additional energy needed to deprotonate weaker acids, resulting in large changes in DPE having relatively small impacts on activation energies $(d(E_{A,R})/d(DPE) = 0.11)$.

Measured selectivities reflected, in part, transport restrictions of product alkenes within acid domains instead of the rate constants for the formation of *individual* products from each reactant. In such cases, selectivities to isomerization products formed from reactant-derived alkenes after only a single sojourn at an acid site cannot be estimated directly from measured selectivities, because secondary interconversions of alkene products are similar in rates to their hydrogenation, both locally within acid domains via hydrogen transfer from alkane reactants or via reactions with H$_2$ after their diffusion through such acid domains to reach Pt sites. The rate constant for the formation of 3MP from 2MP reactants, and consequently the 2MP isomerization selectivity to 3MP and the ratio of this to that for isomerization products that vary backbone length (s_{MS}), were determined explicitly, without the use of measured product selectivities, from mechanism-based interpretations of measured turnover rates for all hexane isomer reactants on each catalyst mixture. Determined s_{MS} values and, consequently, the tendency for alkenes to methyl shift, branch, or chain lengthen were unaffected by the DPE, and thus the acid strength, of POM clusters because of the similar amount and localization of cationic charge at all isomerization transition states.

These findings show unequivocally that the demanding or facile nature of a given reaction, which is a property of the stability of the organic cations at ion-pair transition states, is not necessarily relevant to how these catalytic reactions "sense" acid strength changes; this depends on the amount and localization of cationic charge at such transition states. These concepts suggest changing acid strength will lead to more selective conversions of reactant mixtures only when competing pathways are mediated by transition states with different amount or localization of cationic charge, thus showing that isomerization selectivities, often used to assess acid strength, are inappropriate probes of acid strength in the context proposed by, and used in, the previous literature. Although shown here for isomerization reactions, these concepts apply in general to reactions mediated by ion-pairs at transition states.

Appendix A. Supplementary material

Supplementary data associated with this article can be found, in the online version, at http://dx.doi.org/10.1016/j.jcat.2014.09.005.

References

[1] A. Corma, Chem. Rev. 95 (1995) 559.
[2] M.J. Janik, J. Macht, E. Iglesia, M. Neurock, J. Phys. Chem. C 113 (2009) 1872.
[3] J. Macht, M.J. Janik, M. Neurock, E. Iglesia, J. Am. Chem. Soc. 130 (2008) 10369.
[4] M. Brändle, J. Sauer, J. Am. Chem. Soc. 120 (1998) 1556.
[5] A.J. Jones, R.T. Carr, S.I. Zones, E. Iglesia, J. Catal. 312 (2014) 58.
[6] J. Macht, M.J. Janik, M. Neurock, E. Iglesia, Angew. Chem., Int. Ed. 46 (2007) 7864.
[7] R. Carr, M. Neurock, E. Iglesia, J. Catal. 278 (2011) 78.
[8] J. Macht, R.T. Carr, E. Iglesia, J. Am. Chem. Soc. 131 (2009) 6554.
[9] P. Deshlahra, R.T. Carr, E. Iglesia, Ionic and covalent stabilization of intermediates and transition states in catalysis by solid acids, J. Am. Chem. Soc., submitted for publication.
[10] P.B. Weisz, E.W. Swegler, Science 126 (1957) 31.
[11] M. Guisnet, F. Alvarez, G. Giannetto, G. Perot, Catal. Today 1 (1987) 415.
[12] G.D. Pirngruber, K. Seshan, J. Lercher, J. Catal. 186 (1999) 188.
[13] J.J. Cowan, C.L. Hill, R.S. Reiner, I.A. Weinstock, Inorg. Synth. 33 (2002) 18.

[14] L.C. Baker, T.P. McCutcheon, J. Am. Chem. Soc. 78 (1956) 4503.
[15] L.C. Baker, T.P. McCutcheon, J. Am. Chem. Soc. 72 (1950) 2374.
[16] D.W. Scott, Chemical Thermodynamic Properties of Hydrocarbons and Related Substances: Properties of the Alkane Hydrocarbons, C1 through C10, in the Ideal Gas State from 0 to 1500 K, U.S. Bureau of Mines, Washington, 1974.
[17] C.D. Baertsch, K.T. Komala, Y.-H. Chua, E. Iglesia, J. Catal. 205 (2002) 44.
[18] N. Mizuno, M. Misono, Chem. Rev. 98 (1998) 199.
[19] B.B. Bardin, R.J. Davis, Appl. Catal., A 200 (2000) 219.
[20] M. Janik, B. Bardin, R. Davis, M. Neurock, J. Phys. Chem. B 110 (2006) 4170.
[21] X. Rozanska, P. Sautet, F. Delbecq, F. Lefebvre, S. Borshch, H. Chermette, J.-M. Basset, E. Grinenval, Phys. Chem. Chem. Phys. 13 (2011) 15955.
[22] T. Okuhara, N. Mizuno, M. Misono, Adv. Catal. 41 (1996) 113.
[23] G. Djéga-Mariadassou, M. Boudart, J. Catal. 216 (2003) 89.
[24] R. Madon, M. Boudart, Ind. Eng. Chem. Fundam. 21 (1982) 438.
[25] J. Macht, R.T. Carr, E. Iglesia, J. Catal. 264 (2009) 54.
[26] V.B. Kazansky, Acc. Chem. Res. 24 (1991) 379.
[27] M.A. Natal-Santiago, R. Alcalá, J.A. Dumesic, J. Catal. 181 (1999) 124.
[28] M. Boronat, P. Viruela, A. Corma, J. Phys. Chem. 100 (1996) 16514.
[29] T. Demuth, X. Rozanska, L. Benco, J. Hafner, R.A. van Santen, H. Toulhoat, J. Catal. 214 (2003) 68.
[30] A L.L. East, T. Bucko, J. Hafner, J. Phys. Chem. A 111 (2007) 5945.
[31] R.A. Alberty, C.A. Gehrig, J. Phys. Chem. Ref. Data 14 (1985) 803.